Lithos 227 (2015) 77–93

Contents lists available at ScienceDirect

Lithos

journal homepage: www.elsevier.com/locate/lithos

Pyroxenite-derived Early Cretaceous lavas in the Liaodong Peninsula: Implication for metasomatism and thinning of the lithospheric mantle beneath North China Craton

Chong-Jin Pang [a,e], Xuan-Ce Wang [b], Yi-Gang Xu [a,*], Shu-Nv Wen [c], Yong-Sheng Kuang [d], Lu-Bing Hong [a]

[a] State Key Laboratory of Isotope Geochemistry, Guangzhou Institute of Geochemistry, Chinese Academy of Sciences, Guangzhou 510640, PR China
[b] ARC Centre of Excellence for Core to Crust Fluid Systems (CCFS) and The Institute for Geoscience Research (TIGeR), Department of Applied Geology, Curtin University, GPO Box U1987, Perth, WA 6845, Australia
[c] College of Earth Sciences, Guilin University of Technology, Guilin 541004, PR China
[d] Institute of Geology, Chinese Academy of Geological Sciences, Beijing 100037, PR China
[e] University of Chinese Academy of Sciences, Beijing 100049, PR China

ARTICLE INFO

Article history:
Received 28 September 2014
Accepted 23 March 2015
Available online 1 April 2015

Keywords:
Early Cretaceous
Volcanic rocks
Mantle metasomatism
Garnet pyroxenite
Cratonic destruction
North China Craton

ABSTRACT

The Xiaoling lavas, erupted at ca. 110 Ma in the Liaodong Peninsula, North China, provide vital constraints on the thermochemical state of subcontinental lithospheric mantle (SCLM) during the destruction of the craton. The Xiaoling lavas comprise basalt, andesite and dacite. They are characterized by depletion of high field strength elements (HFSE), enrichment of large ion lithophile elements (LILE) and EM1-like Sr–Nd isotopic compositions ($\varepsilon_{Nd}(t) = -8.7 - -16.0$; $^{87}Sr/^{86}Sr_i = 0.7046–0.7054$), consistent with a derivation from the SCLM. With the exception of TiO_2, the studied samples have major element compositions similar to those of experimentally determined partial melts of volatile-free Mid-Ocean-Ridge Basalt (MORB)-like eclogite at 3–5 GPa, but differ from anhydrous peridotite-derived melts. The olivine phenocrysts of the basaltic samples have high Ni and Fe/Mn, and low Ca contents, which are typical of the olivines crystallized from melts derived from a garnet pyroxenitic mantle source. This suggests that the Xiaoling lavas were derived from a pyroxenitic mantle source, which may have been formed by the solid-state reaction between recycled crustal materials and their surrounding peridotites. The presence of abundant amphibole phenocrysts in the Xiaoling lavas suggests a highly hydrated SCLM in this region. The high Rb/Sr but low initial $^{87}Sr/^{86}Sr$ ratios of the Xiaoling samples require a recent metasomatism in the mantle source, which is most likely related to the Pacific subduction. The genesis of the Xiaoling lavas therefore highlights the important role of water and Pacific subduction in the destruction of the North China Craton.

1. Introduction

It is generally accepted that the ancient (~2.5 Ga), refractory, thick (>200 km) and cold (~40 mW/m^2) lithospheric keel beneath the eastern North China Craton (NCC) was replaced by younger, fertile, thin (<80 km) and hot (>60 mW/m^2) lithospheric mantle from the Mesozoic to the Cenozoic (Fig. 1a; Fan et al., 2000; Gao et al., 2002; Griffin et al., 1998; Menzies et al., 1993; Menzies and Xu, 1998; Xu, 2001), although the geodynamic controls of the lithospheric thinning (cratonic destruction) are still controversial (Gao et al., 2004; Menzies et al., 2007; Niu, 2005; Windley et al., 2010; Wu et al., 2008; Xu, 2001; Zhu et al., 2012b). The destruction of the NCC significantly changed thermochemical state and rheological property of its underlying subcontinental lithospheric mantle (SCLM) (Wu et al., 2008; Xu, 2001; Xu et al., 2009; Zhu et al., 2012b). For instance, Xu (2001) reported that the $\varepsilon_{Nd}(t)$ values of the late Jurassic to recent basalts increased from −20 to +8, consistent with the transition from enriched mantle source to depleted mantle appeared at about 90 to 80 Ma.

Mafic magmas are generated by partial melting of the upper mantle. Their formation and composition are controlled by couples of factors, such as source characteristics, degree of partial melting, mantle potential temperature and lithospheric thickness (Xu et al., 2009). Lithospheric mantle is mainly composed of peridotites (e.g., Yang et al., 2010; Zheng, 2009). Partial melting of peridotites (e.g., Guo et al., 2003) or the melt–peridotite interaction (e.g., Zhang et al., 2002, 2003) has been interpreted as the origin of Mesozoic mafic rocks in the NCC. However, recent geochemical and petrological studies show that pyroxenite/eclogite source may have played an important role in the formation of the Mesozoic to Cenozoic basalts in the NCC as well (Hong et al., 2013; Liu et al., 2008; Xu, 2014; Zeng et al., 2011). In particular, Liu et al. (2008) suggested that the >110 Ma basalts were derived from orthopyroxene/garnet-rich mantle source formed by peridotite–melt/fluid reaction, whereas the <110 Ma basalts were products of clinopyroxene/garnet-rich mantle

* Corresponding author. Tel.: +86 20 85290109; fax: +86 20 8529261.
E-mail address: yigangxu@gig.ac.cn (Y.-G. Xu).

http://dx.doi.org/10.1016/j.lithos.2015.03.022
0024-4937/

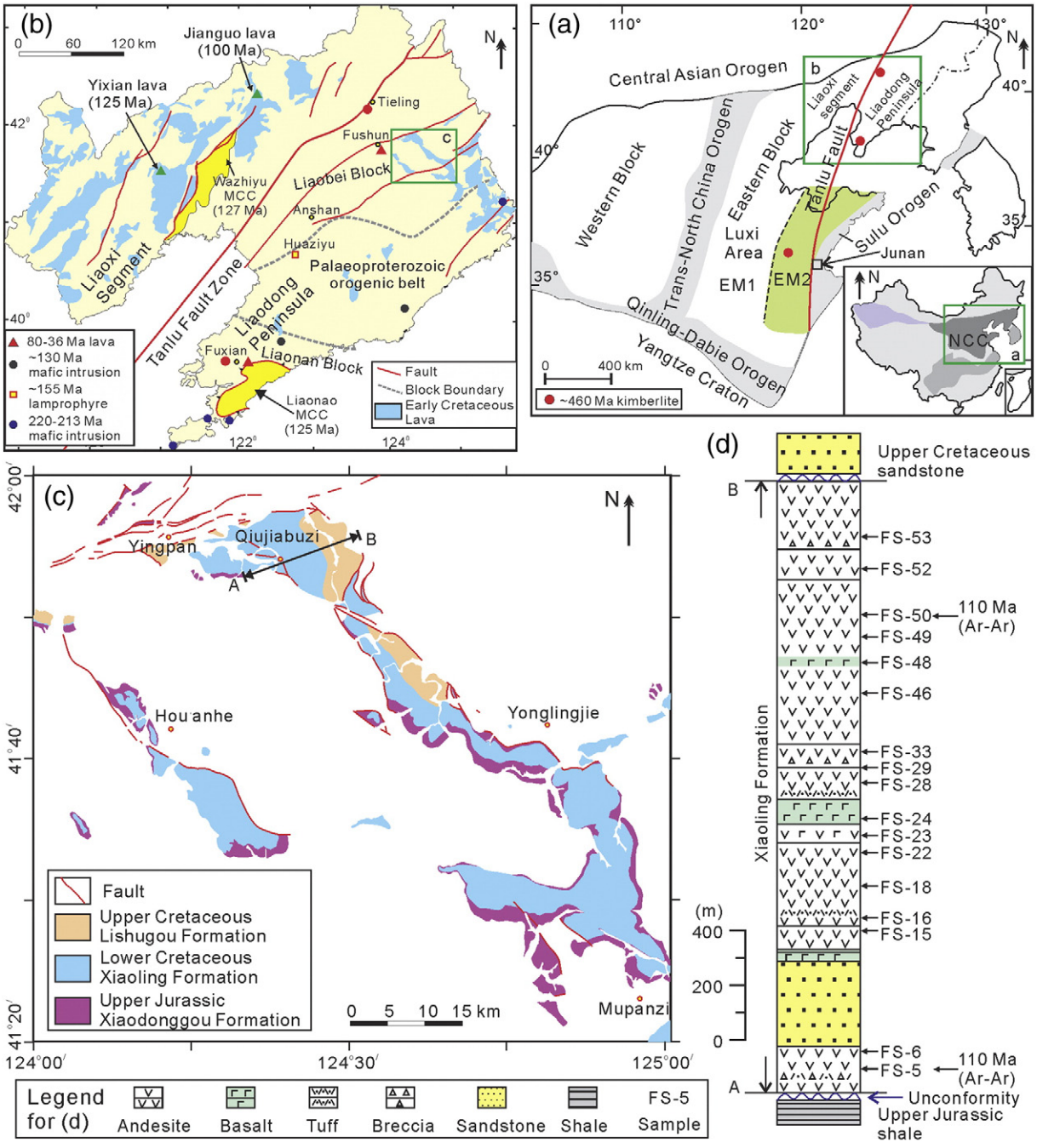

Fig. 1. Geological maps of the study area. (a) Tectonic blocks of China (after Zhu et al., 2012b) and major components of the North China Craton. The boundary between EM1 and EM2 is after Xu et al. (2004). (b) Distribution of the Cretaceous volcano-sedimentary rocks in the Liaoning Province that is separated into the Liaodong Peninsula and the Liaoxi segment by the Tan–Lu Fault Zone. Ages of the lavas, lamprophyre, kimberlite and mafic intrusion are from literatures (Jiang et al., 2005; Kuang et al., 2012; Pei et al., 2011; Wang et al., 2006, 2007; Wu et al., 2006; Yang and Li, 2008; Yang et al., 2007b, 2010, 2012b; Zhang et al., 2003). Location and timing of the Liaonan and Waziyu Metamorphic Core Complex (MCC) are from Zhu et al. (2012a). (c) The Xiaoling Formation and sample locations. (d) The lithology of the Xiaoling Formation (BGMR, 1989) and samples positions (see Fig. 3 for the Ar–Ar age).

source resulted from solid-state mixing of peridotite and rutile-bearing eclogite.

Compared with peridotites, pyroxenites have lower solidus temperature, and thus may significantly contribute to partial melting during pressure release of the adiabatic mantle or thermal erosion of the lithospheric mantle (Herzberg, 2011; Hirschmann and Stolper, 1996; Xu, 2002). In fact, mantle melting may proceed via some combined mechanisms. For example, the addition of volatiles (i.e., H_2O and CO_2), increasing mantle temperature and adiabatic ascent of the asthenosphere subsequent to lithospheric extension can induce partial melting of the mantle (DePaolo and Daley, 2000; McKenzie and Bickle, 1988; Xu et al., 2009). Recent studies demonstrated at least some part of the Mesozoic SCLM beneath the NCC was extremely hydrated with H_2O >1000 ppm by weight during the peak time (~120 Ma) of the NCC destruction (Xia et al., 2013). Thus, the hydration of the SCLM, source characteristics and regional tectonic factors may have controlled the destruction of the NCC.

Paleozoic kimberlites and Mesozoic to Cenozoic mafic magmatism occurred in the Liaodong Peninsula, northeastern NCC (Fig. 1a–b), thus providing vital information related to the evolution of the mantle thermochemical state since the Paleozoic (Griffin et al., 1998; Jiang et al., 2010; Kuang et al., 2012; Liu et al., 2008; Pei et al., 2011; Wang et al., 2006, 2012; Wu et al., 2005a,b, 2006; Yang et al., 2007a,b, 2008b, 2010, 2012b). Studies on mantle xenoliths and mafic to felsic intrusions suggested that the ancient lithospheric mantle had been

replaced by a juvenile lithospheric mantle by ca. 210 Ma beneath this region (Yang et al., 2007b, 2010, 2012b). However, geochemistry of mafic rocks suggested an ancient, isotopically enriched lithospheric mantle during 150–130 Ma (Jiang et al., 2010; Pei et al., 2011), whereas the depleted mantle source became a dominated reservoir since 80 Ma (Kuang et al., 2012; Wang et al., 2006, 2007; Xu, 2014). Thus, it remains ambiguous as to when and how the ancient, enriched mantle was replaced by the young, depleted mantle in this region.

Early Cretaceous volcanic rocks are preserved in the Liaodong Peninsula (Fig. 1b) and bear important information related to the thermochemical evolution of the underlying SCLM. Although the Early Cretaceous marks magmatic climax in the NCC (e.g., Wu et al., 2005a), the genesis of contemporaneous lavas is poorly constrained. In this study, we carried out geochronological, petrological, geochemical and Sr–Nd isotopic analyses for the Early Cretaceous lavas from the Xiaoling Formation in the Liaodong Peninsula, aiming to unravel their magma source and by inference the nature of the SCLM.

2. Geological background and analytical methods

The NCC comprises the Western and Eastern blocks separated by the Trans-North China Orogen formed by the collision between the two blocks during the Palaeoproterozoic (~1.85 Ga) (Fig. 1a; Zhao et al., 2001). The NCC is bounded to the north by the Central Asian orogenic belt and to the south and east by the Qinling–Dabie–Sulu orogenic belt (Fig. 1a). The Central Asian orogenic belt was formed due to the collision between the NCC and the Mongolian microcontinent during the Devonian (Xu et al., 2013), whereas the Qinling–Dabie–Sulu orogenic belt was built by the collision between the NCC and the Yangtze plate during the Late Triassic (Li et al., 1993; Meng and Zhang, 1999).

The Liaodong Peninsula located in the eastern Liaoning Province is separated from the Liaoxi segment (western Liaoning Province) by the Tan–Lu Fault Zone (Fig. 1b). The Liaodong Peninsula consists of the Archean Liaonan Block in the south, the Archean Liaobei Block with ca. 3.8 Ga crust (Liu et al., 1992) in the north, and the Palaeoproterozoic orogenic belt in between (Fig. 1b; Wu et al., 2005b). The Late Triassic intrusions (dolerite, diorite and granite) sporadically spread (Fig. 1b), and were interpreted to mark the onset of magmatism corresponding to the destruction of the craton (Yang et al., 2007b, 2012b). Three stages of granitic magmatism from the Late Triassic to the Early Cretaceous (233–212 Ma; 180–156 Ma; 131–117 Ma) have been recognized in this region, among which the Early Cretaceous magmatism was the most important one (the so-called magmatic climax; Wu et al., 2005a). The Jurassic mafic rocks are rare, with only one identified case for lamprophyres in the Huaziyu area (155 Ma; Jiang et al., 2005, 2010). Mafic to ultramafic intrusive and volcanic rocks (BGMR, 1989; Pei et al., 2011) mostly occurred during the Early Cretaceous, followed by the latest Cretaceous to Eocene basalts (80–36 Ma; Fig. 1b; Kuang et al., 2012; Wang et al., 2006, 2007). Metamorphic core complex of ca. 125 Ma were also developed in the Liaoning Province, implying an extensional setting during the Late Mesozoic (Fig. 1b; Zhu et al., 2012a and references therein).

The studied Xiaoling Formation of 910–3000 m thick outcrops in the Liaobei Block (BGMR, 1989). It is dominated by andesite, along with subordinate amounts of basalt, dacite, andesitic breccia and tuff, and sandstone (Fig. 1d; BGMR, 1989). This formation overlies the Upper Jurassic Xiaodonggou Formation and older strata on an angular unconformity, and is underlain by the Upper Cretaceous Lishugou Formation on a parallel unconformity (Fig. 1d; BGMR, 1989). It has been suggested that the Xiaoling Formation was deposited during the Early Cretaceous based on fossil assemblage (*Acanthopteris gothani–Ruffordia goepperti*) (BGMR, 1989). Lava samples were collected along outcrops from the lower to the upper parts of the Xiaoling Formation corresponding to samples FS-5 to FS-53 (Fig. 1d).

Major and trace elements, Ar/Ar and Sr/Nd isotopic analyses were carried out in the State Key Laboratory of Isotope Geochemistry, Guangzhou Institute of Geochemistry, Chinese Academy of Sciences, whereas major element analyses of minerals were carried out in the Guangxi Key Laboratory of Hidden Metallic Ore Deposits Exploration, Guilin University of Technology (see Appendix 1 for analytical methods and Tables A1–A6, and Appendix 2 for supplementary Figures A1–A5).

3. Petrography

Samples include basalt, andesite and dacite, most of them are porphyritic (<15% phenocrysts). The phenocryst assemblage in basaltic samples mainly comprises olivine, clinopyroxene, together with rare plagioclase. Groundmass is dominated by microlitic clinopyroxene and plagioclase, along with rare apatite and Fe–Ti oxides (Fig. 2). Most olivine phenocrysts in the basaltic samples (i.e., FS-24 and FS-48) are partly altered, whereas fresh olivine phenocrysts are mostly euhedral to subhedral, ranging from 0.1 to 0.6 mm in size (Fig. 2a, c). Some olivine crystals were completely altered but preserved as pseudomorph of olivine (Fig. 2a). Clinopyroxene phenocrysts are present as single crystals or aggregates, and are from 0.07 to 0.8 mm in length (Fig. 2d). Common inclusions in clinopyroxene are microlitic apatite and Fe–Ti oxides (Fig. 2d).

The phenocryst assemblage in andesitic samples is composed of clinopyroxene (and amphibole), along with rare plagioclase and quartz (Fig. 2b). The groundmass mainly consists of microlitic plagioclase and clinopyroxene. Zoned clinopyroxene phenocrysts are present in some andesitic samples, and comprise a partly altered, euhedral to anhedral grzy core and a darker grzy rim. Amphibole occurs as major phenocrysts in some andesitic samples, and is euhedral with a grain size of 0.1 to 0.4 mm. They are generally surrounded by an opacitized or partly altered rim of variable thickness (Fig. 2b). In addition, quartz phenocrysts occasionally occur in some andesitic samples, and are always embayed (Fig. 2b).

The phenocryst assemblage in dacitic samples mainly consists of amphibole, plagioclase, together with a few clinopyroxene and quartz. Plagioclase phenocrysts is present as single crystals or aggregates varying from 0.1 to >0.5 mm in length. Amphibole phenocrysts are generally euhedral, and are 0.5 to 1 mm in grain size. Quartz phenocrysts commonly occur in dacitic samples, and are embayed in shape with a grain size of 0.1 to 0.8 mm.

4. Analytical results

4.1. Ar–Ar geochronology

As shown in Fig. 3, $^{40}Ar/^{39}Ar$ dating results of two samples (FS-5 and FS-50) are plotted as age spectrum and $^{40}Ar/^{36}Ar$–$^{39}Ar/^{36}Ar$ isotope correlation diagrams. Details of results are present in Table A1. All errors are reported at the 2σ level. Sample FS-5 collected from the lower part of the Xiaoling Formation (Fig. 1d) yields a weighted plateau age of 110.5 ± 1.1 Ma (MSWD = 1.33), corresponding to 62% of total released ^{39}Ar (Fig. 3). The isochron diagram shows that the initial $^{40}Ar/^{36}Ar$ ratio is 276.2 ± 12.9, close to the present atmospheric $^{40}Ar/^{36}Ar$ ratio (295.5), implying that the excess argon is insignificant. Furthermore, the normal isochron age of sample FS-5 is 111.1 ± 1.2 Ma (MSWD = 0.16), identical with its weighted plateau age within error. Therefore, the plateau age (110.5 ± 1.1 Ma) is interpreted to be the eruption age for the lower part of the Xiaoling Formation.

Sample FS-50 collected the upper part of the Xiaoling Formation (Fig. 1d) has a weighted plateau age of 110.4 ± 0.7 Ma (MSWD = 3.68), corresponding to 80% of total released ^{39}Ar (Fig. 3). The initial $^{40}Ar/^{36}Ar$ ratio is of 335 ± 107, consistent with the present atmospheric $^{40}Ar/^{36}Ar$ ratio (295.5) within error. The normal isochron age of sample FS-50 is 108.8 ± 4.3 Ma (MSWD = 3.61), close to the weighted plateau age. Collectively, the Xiaoling lavas were erupted at about 110 Ma, consistent with the bio-stratigraphic data.

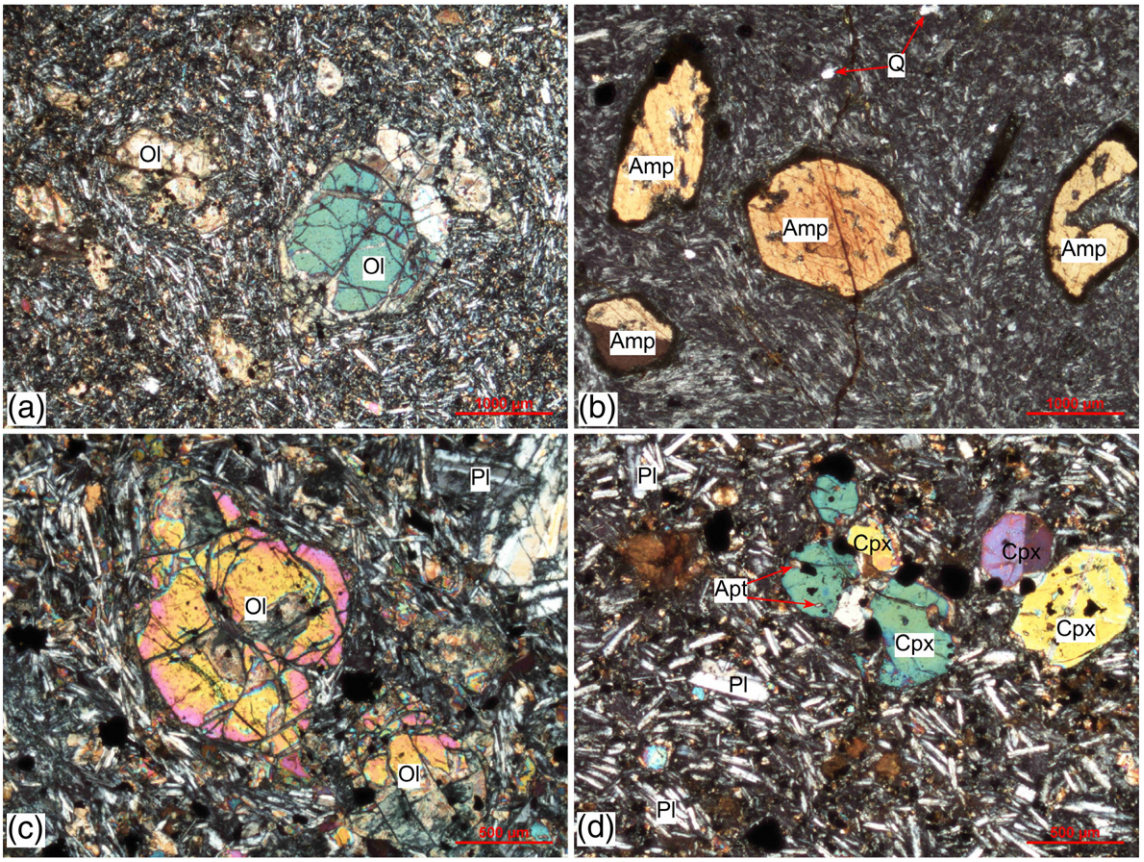

Fig. 2. Photograph of thin sections in selected samples. (a) Olivine (Ol) phenocrysts in FS-24. (b) Amphibole (Amp) and Quartz (Q) in FS-29. (c) Plagioclase (Pl) and zone olivine in FS-48. (d) Clinopyroxene (Cpx) with Apatite (Apt) inclusions, and plagioclase in FS-50.

4.2. Major and trace elements

Most of the Xiaoling lavas have relatively low LOI values of <3.0 wt.% (Table A2). According to the nomenclature of Le Bas et al. (1986), the Xiaoling lavas are dominated by basaltic trachyandesite and trachyandesite, accompanied by basalt, andesite and dacite, plotting within the alkaline (9 samples) and subalkaline (8 samples) fields, without bimodal characteristic (Fig. 4). However, the subalkaline

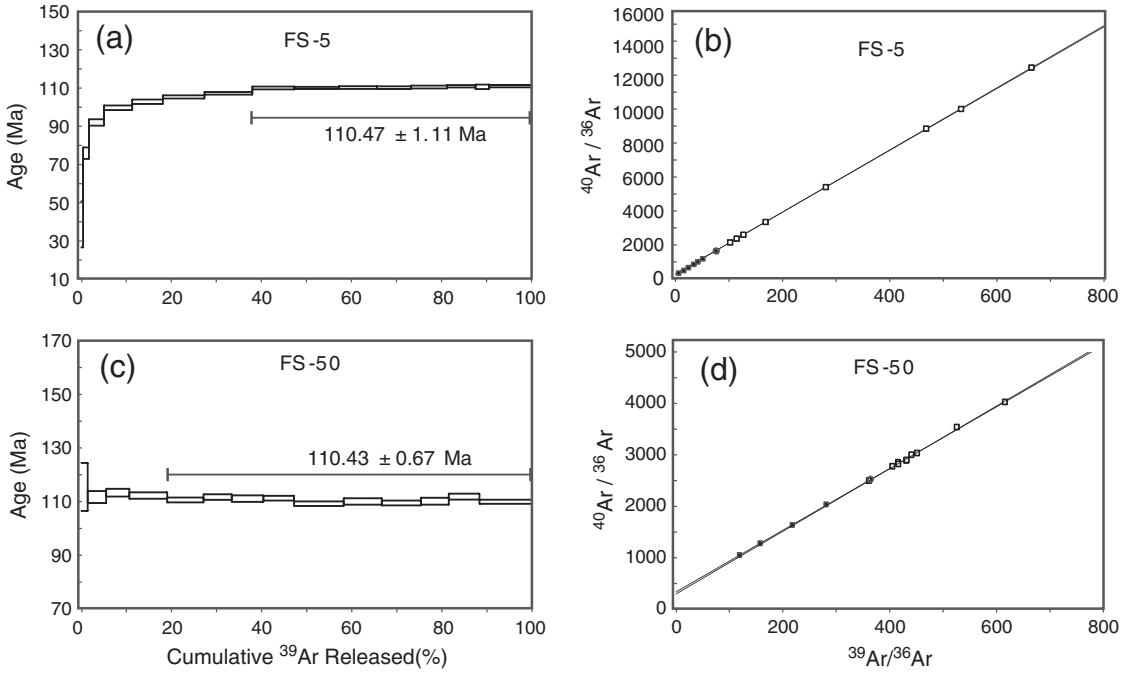

Fig. 3. $^{40}Ar/^{39}Ar$ dating results of the Xiaoling lavas, showing an erupted age of 110 Ma. Sample FS-5 is from the lower part of the section, whereas FS-50 from the upper part.

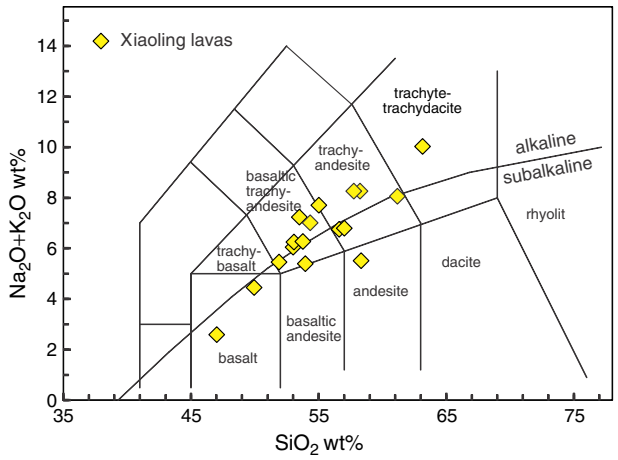

Fig. 4. TAS diagram for rock type classification (after Le Bas et al., 1986). Major elements of samples with amphibole phenocrysts (FS-6, -28, -29 and -46) were not normalized to 100% by volatile-free, whereas major elements of other samples were normalized.

and alkaline series according to geochemical classification do not show any significant petrographic distinction. Samples have a wide range of SiO_2 (45.4–62.0 wt.%), MgO (1.2–9.2 wt.%), and $Fe_2O_3^t$ (4.6–12.9 wt.%), with Mg# from 33 to 64 [Mg# = 100 × Mg/(Mg + Fe^{2+}) atomic ratio] (Table A2). They are characterized by higher Al_2O_3 (14.8–17.3 wt.%) but lower TiO_2 (0.66–1.52 wt.%) relative to those of Cenozoic basalts in the NCC (not shown). Samples show a medium-K to shoshonitic affinity with K_2O contents ranging from 0.55 to 3.42 wt.% (Table A2; Fig. 5). As shown in Fig. 5, samples display negative correlations of TiO_2, $Fe_2O_3^t$, MgO, CaO and MnO with SiO_2, but positive correlations of Na_2O, K_2O, and Al_2O_3. P_2O_5 contents firstly increase until SiO_2 = 53 wt.%, but decrease with increasing of SiO_2 (Fig. 5).

Samples have a wide range of Ni (1.7–181.4 ppm) and Cr (7.4–322.5 ppm) contents, negatively correlating with SiO_2 (Table A2; Fig. A1). Niobium (Nb) concentration varies from 9.63 to 20.14 ppm (Table A2; Fig. A1). Scandium (Sc) concentration varies from 5.52 to 24.66 ppm negatively correlating with SiO_2 (Table A2; Fig. A1). All samples exhibit similar chondrite-normalized rare earth element (REE) patterns, with enrichment of light REE (LREE) over heavy REE (HREE) ($(La/Yb)_N$ = 8.7–38.42; Fig. 6), without significant Eu anomalies (Eu/Eu^* = 0.97–1.21; Fig. 6). In primitive mantle-normalized trace element patterns (Fig. 6), samples all show enrichment in large ion lithophile elements (LILE, such as Rb, Ba, K, Pb and Sr), but depletion in high field strength elements (HFSE, such as Nb, Ta, Ti, Zr and Hf) relative to neighboring elements, compared with those of ~130 Ma basalts in the Luxi area in the interior of the NCC (Fig. 6; Guo et al., 2003).

4.3. Sr–Nd isotopes

The Xiaoling lavas have variable $\varepsilon_{Nd}(t)$ values, varying from −8.7 to −16.0, but relatively uniform initial $^{87}Sr/^{86}Sr$ ratios, ranging from 0.7046–0.7054 (Table 1). In $\varepsilon_{Nd}(t)$ vs. $^{87}Sr/^{86}Sr_{initial}$ diagram (Fig. 7), all samples are plotted within the EM1 field (enriched mantle component with low $^{143}Nd/^{144}Nd$ and intermediate $^{87}Sr/^{86}Sr$ ratios; Zindler and Hart, 1986), similar to those of the ~130 Ma gabbros and basalts in the Luxi area (Figs. 1a, 7; Guo et al., 2001, 2003; Huang et al., 2012). However, Sr–Nd isotopic compositions of our samples are distinguishable from those of the Jurassic lamprophyres ($^{87}Sr/^{86}Sr_i$ = 0.7075–0.7121, $\varepsilon_{Nd}(t)$ = −14.3–−−1.9; Jiang et al., 2010), and Triassic mafic intrusions ($^{87}Sr/^{86}Sr_i$ = 0.7063–0.7160, $\varepsilon_{Nd}(t)$ = −14.8–−1.3; Yang et al., 2007b) and Cretaceous mafic intrusions ($^{87}Sr/^{86}Sr_i$ = 0.7056–0.7111, $\varepsilon_{Nd}(t)$ = −20–−5.5; Pei et al., 2011) in the Liaodong Peninsula (Fig. 7). They are also different from those of the 80–36 Ma basalts in the Liaodong Peninsula and the ca. 100 Ma basalts in the Liaoxi region (Figs. 1b and 7; Kuang et al., 2012; Wang et al., 2006, 2007; Zhang et al., 2003).

4.4. Mineral compositions

4.4.1. Olivine

Olivine phenocrysts in high-Mg samples (i.e., FS-24 and FS-48) have a wide range of Fo values [Fo = 100 × Mg/(Mg + Fe), cation ratio] varying from 58.9 to 87.3 (Table A3; Fig. 8a). MnO and CaO contents are negatively correlated with Fo values, whereas NiO content is positively correlated with Fo values. All olivine phenocrysts have higher CaO contents (0.1–0.47 wt.%) than those of mantle xenoliths (typically CaO <0.1 wt.%; Table A3; Thompson and Gibson, 2000; Xu and Bodinier, 2004). Most olivine phenocrysts of FS-48 are zoned, whereas zoned olivines are rare in FS-24 (Figs. 2, 8b–c). These zoned olivines commonly have decreasing Fo values and NiO contents, but increasing FeO^t contents from the core to the rim (Fig. 8d). MnO and CaO contents generally increase with decreasing Fo values from the core via the mantle to the rim in the zoned olivine phenocrysts of FS-48.

4.4.2. Clinopyroxene

Chemical compositions of the analyzed clinopyroxenes (Cpx) are presented on Table A4. Cations were calculated on a six-oxygen basis following the program of Sturm (2002), and ferric iron was calculated using the charge balance method. A few Cpx phenocrysts in high-SiO_2 (>54 wt.%) samples show oscillatory zoning and compositional variations (such as MgO, Al_2O_3 and FeO^t) from the core to the rim (not shown). Although complex zoning in some Cpx phenocrysts, all the analyses in cores and rims fall in the diopside to Mg-augite field in terms of En-Fs-Wo nomenclature with end-member compositions of $En_{36–48}Fs_{9.9–18.2}Wo_{40.6–48.6}$ (Fig. 9). All clinopyroxenes are plotted within the Ca–Mg–Fe pyroxene (Quad area) field in the Q–J diagram (Fig. 9). Their Mg# values range from 67.5 to 83.2. FeO^t contents of Cpx phenocrysts correlate negatively with Mg#, whereas SiO_2, TiO_2, Al_2O_3, CaO, Na_2O, and MnO do not systematically correlate with Mg# (Fig. A2).

4.4.3. Amphibole

Amphiboles were not observed in low-SiO_2 (<54 wt.%) samples, whereas they are abundant in high-SiO_2 (>54 wt.%) samples. They are rich in MgO (13–15 wt.%), FeO^t (10.8–13.3 wt.%), CaO (10.6–11.6 wt.%) and Al_2O_3 (10–13 wt.%) with minor amounts of TiO_2 (0.5–3.3 wt.%), Na_2O (2.5–3.2 wt.%) and K_2O (0.6–0.8 wt.%), compared with those of amphiboles in calc-alkaline magma (Table A5; Fig. 10a–c; Ridolfi et al., 2010). TiO_2 contents concentrate at 0.52–0.85 wt.% and 1.88–3.26 wt.%. According to Leake et al. (1997), these amphiboles can be classified as magnesiohastingsite (one edenite). Amphiboles have low Al# [Al# = $Al^{vi}/(Al^{vi} + Al^{iv}) \leq 0.21$] resembling those of amphiboles in calc-alkaline magma (Fig. 10d; Ridolfi et al., 2010). The calculated temperatures of magma are from 902 to 968 °C (±22 °C), and water contents of the equilibrated melt (H_2O_{melt}) are between 3.9 and 6.5 wt.% (±0.6 and ± 1.0 wt.%, respectively; Fig. 10e–f) using amphibole thermobarometer of Ridolfi et al. (2010).

4.4.4. Feldspar

Plagioclases presented as phenocrysts and microlitic phases were analyzed (Table A6). Plagioclases in low-SiO_2 sample (FS-48) have high Al_2O_3 (27.3–29.6 wt.%) and CaO (10.4–13.4 wt.%), low Na_2O (4.4–4.8 wt.%) contents, whereas those in high-SiO_2 sample (FS-46) have high Na_2O (10.7–11.2 wt.%), medium Al_2O_3 (19.1–19.4 wt.%), low CaO (0.1–0.3 wt.%) contents. Thus, plagioclases in low-SiO_2 sample can be classified as labradorite ($An_{53.5–61.9}Ab_{36.8–44.5}Or_{1.4–2.0}$), whereas those in high-SiO_2 sample are albite ($An_{0.4–1.4}Ab_{98.2–99.2}Or_{0.15–0.38}$).

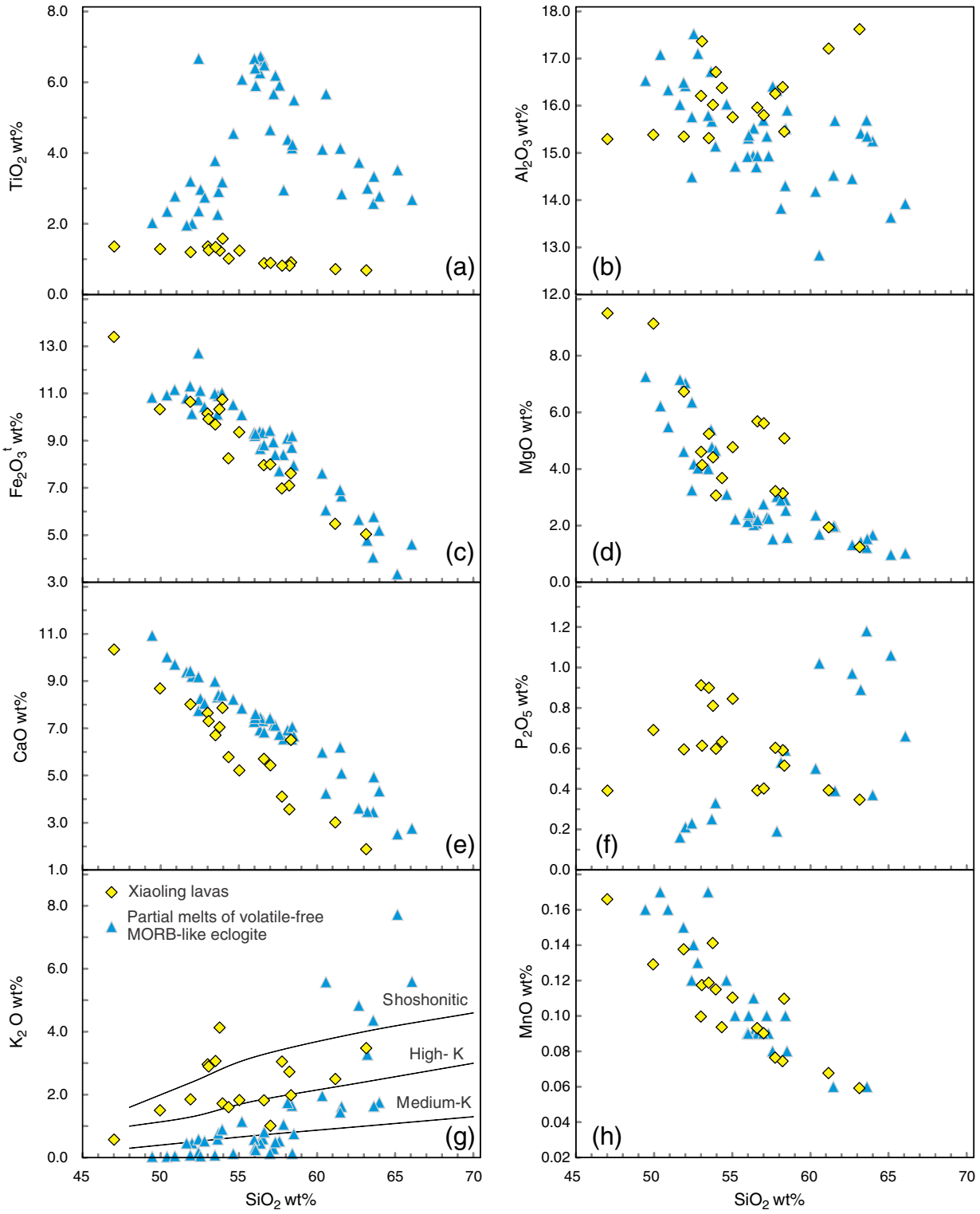

Fig. 5. Major elements vs. SiO_2 diagrams. Partial melts of volatile-free MORB-like eclogite at 3–5 GPa were cited from Pertermann and Hirschmann (2003) and Spandler et al. (2008).

5. Discussion

5.1. Effects of alteration and crystal fractionation

In order to reveal the characteristics of the parental magma source, we examine possible effects of alteration, crustal contamination and crystal fractionation on whole-rock geochemical composition. Measured samples of the Xiaoling lavas have relatively low LOI (<3.0 wt.%; Table A2), although the alteration of phenocrysts or groundmass can be observed (Fig. 2). Negative correlation between K_2O and LOI implies that K was possibly mobile during alteration (Fig. A3), whereas the lack of correlation between LOI and other major elements indicates that they were essentially immobilized.

Zirconium (Zr) is suggested to be immobile during low-grade metasomatism and alteration, and can be used as an alteration-independent index of geochemical variation for basaltic rocks (Polat et al., 2002;

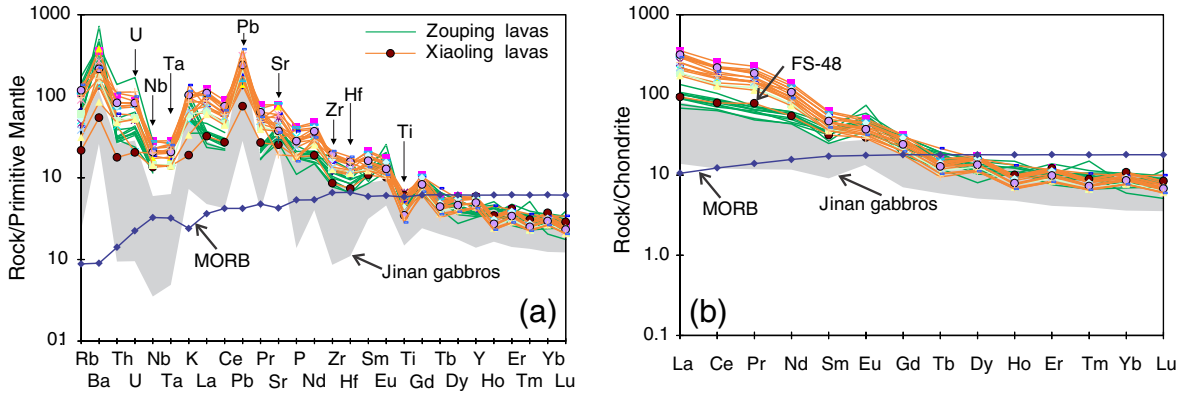

Fig. 6. Chondrite-normalized REE pattern and Primitive mantle-normalized incompatible trace element patterns. Data sources: Normalized values and N-MORB (Sun, and McDonough, 1989); the Zouping lavas (Guo et al., 2003); the Jinan gabbros (Huang et al., 2012).

Wang et al., 2008, 2010). Thus, bivariate plots of Zr vs. selected trace elements can be used to evaluate mobility of such elements during alteration. For the Xiaoling lavas, REE, HFSE (Nb, Ta, Ti and Hf), Lu, Rb, Th, U, Ni, Cr and Sc correlate with Zr (Fig. A4), implying that these elements were essentially immobile during alteration (Wang et al., 2008). Consistency of trace elements and isotopic compositions (Figs. 6, 7), together with lack of secondary minerals also excludes significant alteration. In summary, alteration only played minor roles in whole-rock chemical compositions of the Xiaoling lavas.

All samples are characterized by relatively high SiO_2 (45.4–62 wt.%), but low MgO (1.2–9.2 wt.%), Cr (7.4–322.5 ppm) and Ni (1.7–181.4 ppm) contents. Although both mantle melting and fractional crystallization processes could cause such variations, the depletion of MgO, Ni and Cr in the studied samples suggests that they are not in equilibrium with mantle peridotites (Wang et al., 2012, 2014) and may have experienced fractional crystallization. Negative correlations between MgO, CaO, Ni, Cr, Sc and SiO_2 (Figs. 5, A1) indicate that the fractionation of olivine and clinopyroxene played an important role in magma evolution. Besides, negative correlations between TiO_2, $Fe_2O_3^t$, P_2O_5 and SiO_2 (Fig. 5) are attributable to the fractionation of Ti–Fe minerals and apatite. The fractionation of apatite is consistent with slightly negative P anomaly (Fig. 6) and the positive correlation between Sr and MREE (Tb and Dy) (not shown). Lack of Eu anomaly (Fig. 6) implies that the fractionation of plagioclase is insignificant. Therefore, the parental magma of the Xiaoling lavas underwent the fractionation of olivine, clinopyroxene, Ti–Fe minerals and apatite.

5.2. Crustal contamination

Crustal contamination is inevitable for mantle-derived melts when they ascend through continental crust (DePaolo, 1981; Spera and Bohrson, 2001) and can be identified by the correlation between indices of fractionation and chemical/isotopic data (Wang et al., 2008, 2013). High-SiO_2 samples have nearly constant $^{87}Sr/^{86}Sr_{initial}$ ratios and $\varepsilon_{Nd}(t)$ values, and have no significant correlation between SiO_2, Mg#, Th/La and $\varepsilon_{Nd}(t)$ values (Figs. 11, A5), ruling out significant crustal contamination during magma ascending. In contrast, low-SiO_2 samples show negative correlations of $\varepsilon_{Nd}(t)$ with SiO_2 and Th/La, and positive correlation of Mg# with Nb/La (Figs. 11, A5), implying that they had undergone crustal contamination. These low-SiO_2 lavas have low $^{87}Sr/^{86}Sr_{initial}$ ratios and negative $\varepsilon_{Nd}(t)$ values (Fig. 7), showing a trend toward those of ancient lower crust of the NCC (e.g., Jahn, et al., 1999). In addition, they are relatively depleted in Th and U, especially samples FS-24 and FS-48 (Fig. 6). We therefore suggest that crustal contaminated agent is most likely to be ancient lower crust of the NCC, rather than the upper crust.

The Mesozoic mafic rocks in the Luxi area in the interior of the NCC have $^{87}Sr/^{86}Sr_{(110\ Ma)}$ of 0.7040–0.7065, and $\varepsilon_{Nd}(110\ Ma)$ of −4.2–−16.4 (Fig. 7), typical characteristics of those derived from the enriched SCLM (Guo et al., 2001, 2003; Huang et al., 2012; Zhang et al., 2004). The Sr–Nd isotopic compositions of the Xiaoling lavas are identical to those of the Luxi mafic rocks (Fig. 7; Table 1). Moreover, both the less-evolved Xiaoling lavas (e.g., FS-48 with MgO = 9.2 wt.%) and the Luxi mafic rocks have similar trace element compositions (enrichment of LILE and depletion of HFSE; Fig. 6). These imply that they might have been derived from similar mantle sources. The correlation between SiO_2, Th/La, Nb/La and $\varepsilon_{Nd}(t)$ also points to an end-member component with elevated $^{143}Nd/^{144}Nd$ and Nb/La, but low Th/La values similar to those of mantle source represented by the Luxi mafic rocks (Figs. 7, 11). It is thus reasonable to assume a source component with $^{87}Sr/^{86}Sr$ of 0.7040 and $^{143}Nd/^{144}Nd$ of 0.5122 ($\varepsilon_{Nd} = -6$; Fig. 7) to represent the primary magmas of the Xiaoling lavas.

The Energy-Constrained AFC model (EC-AFC) (Bohrson and Spera, 2001; Spera and Bohrson, 2001) was applied to further investigate the thermal, isotopic and chemical relationship between the crust materials, the assumed primary magma and the Xiaoling lavas. Sr and Nd concentrations for the NCC lower crust ($^{87}Sr/^{86}Sr = 0.710$; $^{143}Nd/^{144}Nd = 0.511$) are 300 ppm and 24 ppm, respectively, as

Table 1
Sr–Nd isotopic compositions of the Xiaoling lavas.

Sample	$^{87}Rb/^{86}Sr$	$^{87}Sr/^{86}Sr$ (2σ)	$(^{87}Sr/^{86}Sr)_i$	$^{147}Sm/^{144}Nd$	$^{143}Nd/^{144}Nd$ (2σ)	$(^{143}Nd/^{144}Nd)_i$	$\varepsilon_{Nd}(t)$	T_{DM} (Ma)
FS-5	0.1466	0.705273±4	0.7050	0.0995	0.511894±7.2	0.5118	−13.1	1682
FS-16	0.0746	0.704707±4	0.7046	0.0969	0.511826±9.0	0.5118	−14.4	1732
FS-18	0.1244	0.705330±7	0.7051	0.0895	0.511892±8.8	0.5118	−13.0	1548
FS-23	0.0728	0.705318±5	0.7052	0.0938	0.511866±7.8	0.5118	−13.6	1637
FS-24	0.1020	0.705286±5	0.7051	0.0895	0.512026±9.2	0.5120	−10.4	1384
FS-28	0.1326	0.705587±5	0.7054	0.0853	0.511770±9.6	0.5117	−15.4	1643
FS-46	0.4356	0.705563±4	0.7049	0.0874	0.511825±8.2	0.5118	−14.3	1604
FS-48	0.0746	0.705182±4	0.7051	0.1148	0.512132±6.8	0.5120	−8.7	1574
FS-53	0.3343	0.705884±4	0.7054	0.0860	0.511792±7.8	0.5117	−14.9	1626
FS-50	0.0602	0.705140±17	0.7050	0.0977	0.511744±10	0.5117	−16.0	1853

All errors are 2σ internal precision at the last significant digit. The initial isotopic ratios are calculated at 110 Ma, using relevant element concentration measured by ICP-MS.

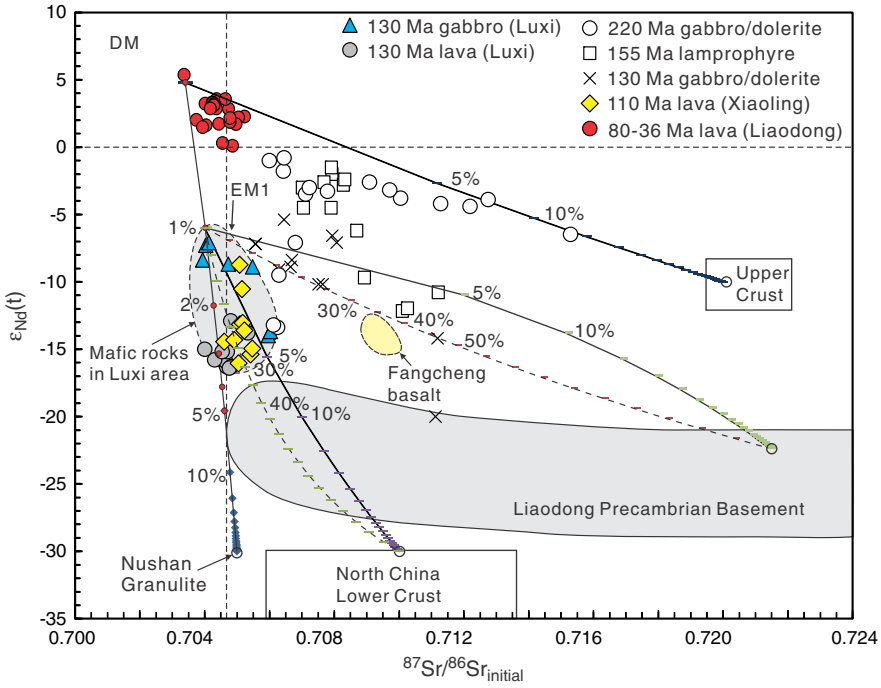

Fig. 7. Sr–Nd isotopic compositions of the Xiaoling lavas. Data sources: 220 Ma mafic intrusions (Yang et al., 2007b, 2012b); 155 Ma lamprophyres (Jiang et al., 2010); 130 Ma mafic intrusions (Pei et al., 2011), 130 Ma mafic rocks in the Luxi area (Guo et al., 2003; Huang et al., 2012); 125 Ma Fangcheng basalts (Zhang et al., 2002); 80–36 Ma basalts (Kuang et al., 2012; Wang et al., 2006, 2007); upper and lower crust of North China (Jahn, et al., 1999); Nushan granulite (Huang et al., 2012); Liaodong Precambrian Basement (Wu et al., 2005b). DM and EM1 are after Zindler and Hart (1986). Mixing models for source (solid line) and melt assimilation (dash line) are also shown. Parameters are assumed as followed:

	$^{87}Sr/^{86}Sr$	Sr (ppm)	ε_{Nd}	Nd (ppm)	Reference
Asthenospheric source	0.7034	21	4.78	1.35	Huang et al. (2012)
Nushan granulite	0.705	1250	−30	60	Huang et al. (2012)
Lower crust of NCC	0.710	300	−30	24	Jahn et al. (1999)
Upper crust of NCC	0.720	350	−10	26	Jahn et al. (1999)
Liaodong Basement	0.7214	531	−22	16	Wu et al. (2005b)

suggested by Jahn, et al. (1999). Variable Sr and Nd contents exhibited by the Luxi mafic rocks and the Xiaoling lavas are examined to fit the wide range of Nd concentrations. The physical and thermal parameters for the magma–wallrock system are close to those of Bohrson and Spera (2001) (Table 2). The best fit models indicate that the involvement ratios of lower crustal materials in magma body were less than 0.175 (mostly ≤0.117, total mass of melted wallrock normalized to original mass of magma body; Fig. 11e–f). In particular, the melted crustal materials in parental magma of FS-48 could be between 0.015 and 0.039, whereas <0.063 for FS-24 (Fig. 11e–f), implying insignificant crustal contamination.

As mentioned above, the Xiaoling lavas consist of basalt, andesite and dacite, showing no bimodal feature. All samples were collected from a continuously exposed outcrop, where basaltic and dacitic rocks are interbedded with andesitic rocks. The Ar–Ar geochronological results constrain that the Xiaoling lavas were emplaced in a relatively short geological interval. Basaltic samples are characterized by undersaturated silicate contents (SiO_2 = 45–53.6 wt.%), relatively high TiO_2 (1.2–1.5 wt.%), MgO (4.0–8.9 wt.%), CaO (5.1–10 wt.%), Ni (28–181 ppm), and Cr (31–322.5 ppm) contents (Table A2), consistent with those of partial melts derived from a mantle source. Andesitic and dacitic samples exhibit saturated to oversaturated silica contents, and are depleted in CaO (1.8–6.4 wt.%), MgO (1.2–5.5 wt.%), TiO_2 (0.66–1.1 wt.%), Ni (1.7–102 ppm), and Cr (7.4–175 ppm) (Table A2). However, all samples are characterized by pronounced HFSE depletion, LILE and LREE enrichment, and EM1-like Sr–Nd isotopic ratios (Figs. 6, 7). All these information imply that all samples shared a similar mantle source. As discussed above, basaltic samples underwent AFC processes during magma ascending, whereas andesitic and dacitic samples were

Table 2
Physical and chemical parameters of EC-AFC modeling.

	Sr	Nd
Compositional paremeters		
Magma isotope ratios	0.704	0.5122
Magma trace element partition coefficient	1.5	0.25
Assimilant initial concentrations (ppm)	300	24
Assimilant isotope ratios	0.71	0.511
Assimilant trace element partition coefficient	1.5	0.25
Source 1		
Magma initial concentrations (ppm)	650	12
Source 2		
Magma initial concentrations (ppm)	500	15
Source 3		
Magma initial concentrations (ppm)	450	19
Source 4		
Magma initial concentrations (ppm)	350	27
Thermal parameters		
Magma liquid temperature, T_l^m (°C)	1300	
Magma initial temperature, T_m^0 (°C)	1300	
Assimilant liquids temperature, T_l^a (°C)	1000	
Assimilant initial temperature, T_a^0 (°C)	300	
Solidus temperature, T_s (°C)	850	
Equilibration temperature, T_{eq} (°C)	930	
Isobaric specific heat of magma, $C_{p,m}$ (J/Kg per K)	1484	
Isobaric specific heat of assimilant, $C_{p,a}$ (J/Kg per K)	1388	
Crystallization enthalpy, Δhcry (J/Kg)	396,000	
Fusion enthalpy, Δhfus (J/Kg)	354,000	

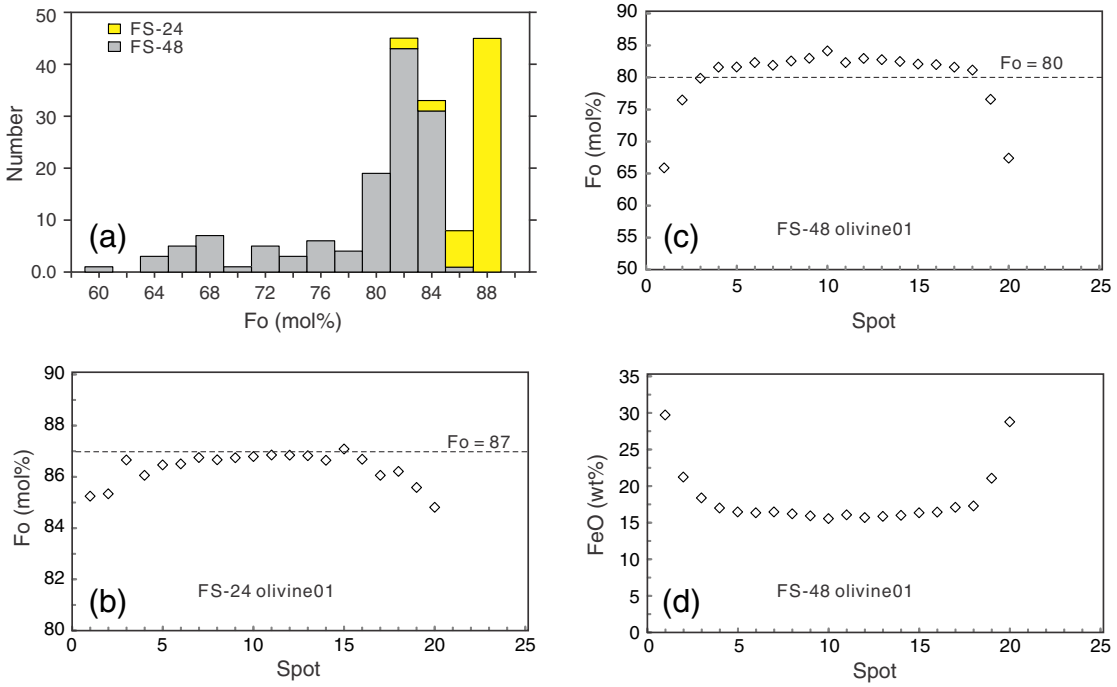

Fig. 8. Compositional variations of olivine phenocrysts in the Xiaoling lavas. (a) Fo histogram of olivine phenocrysts. Representative profiles from the rim to the core to the rim for (b) Fo values of a zoned olivine in FS-24, (c) for Fo values of a zoned olivine in FS-48, and (d) for FeO^t contents of a zoned olivine in FS-48.

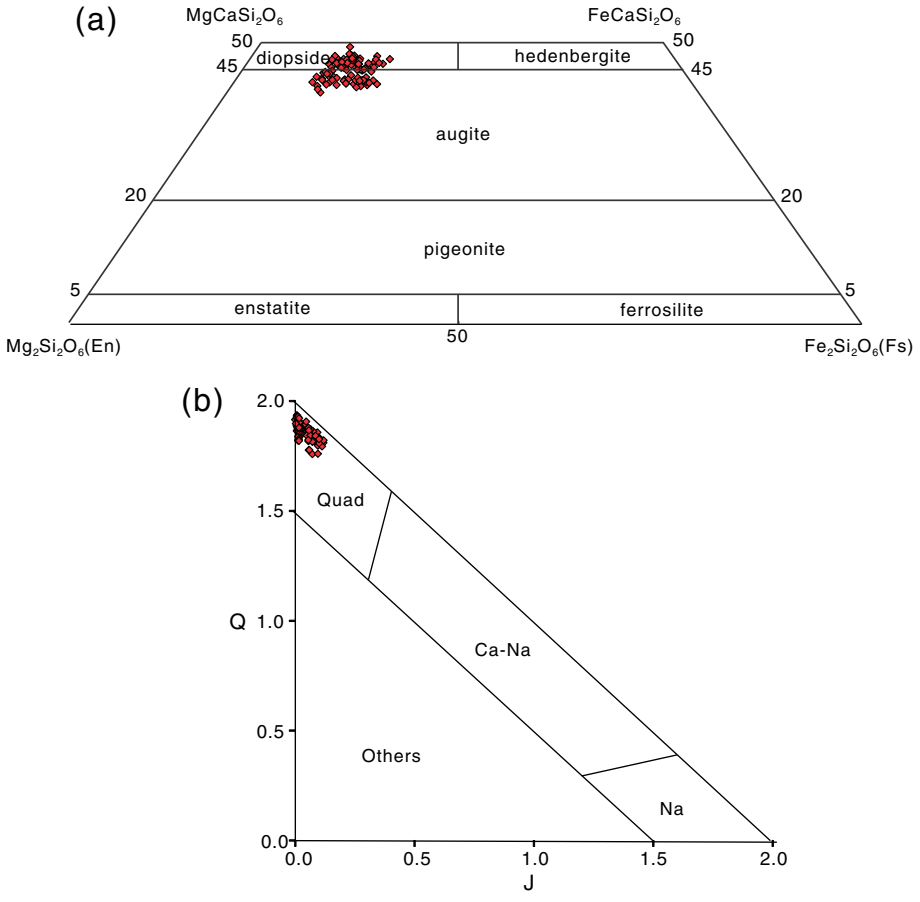

Fig. 9. Compositional variations of clinopyroxenes. (a) The pyroxene quadrilateral. (b) Q–J diagram. Abbreviations and compositions of the end-members are after Morimoto (1988).

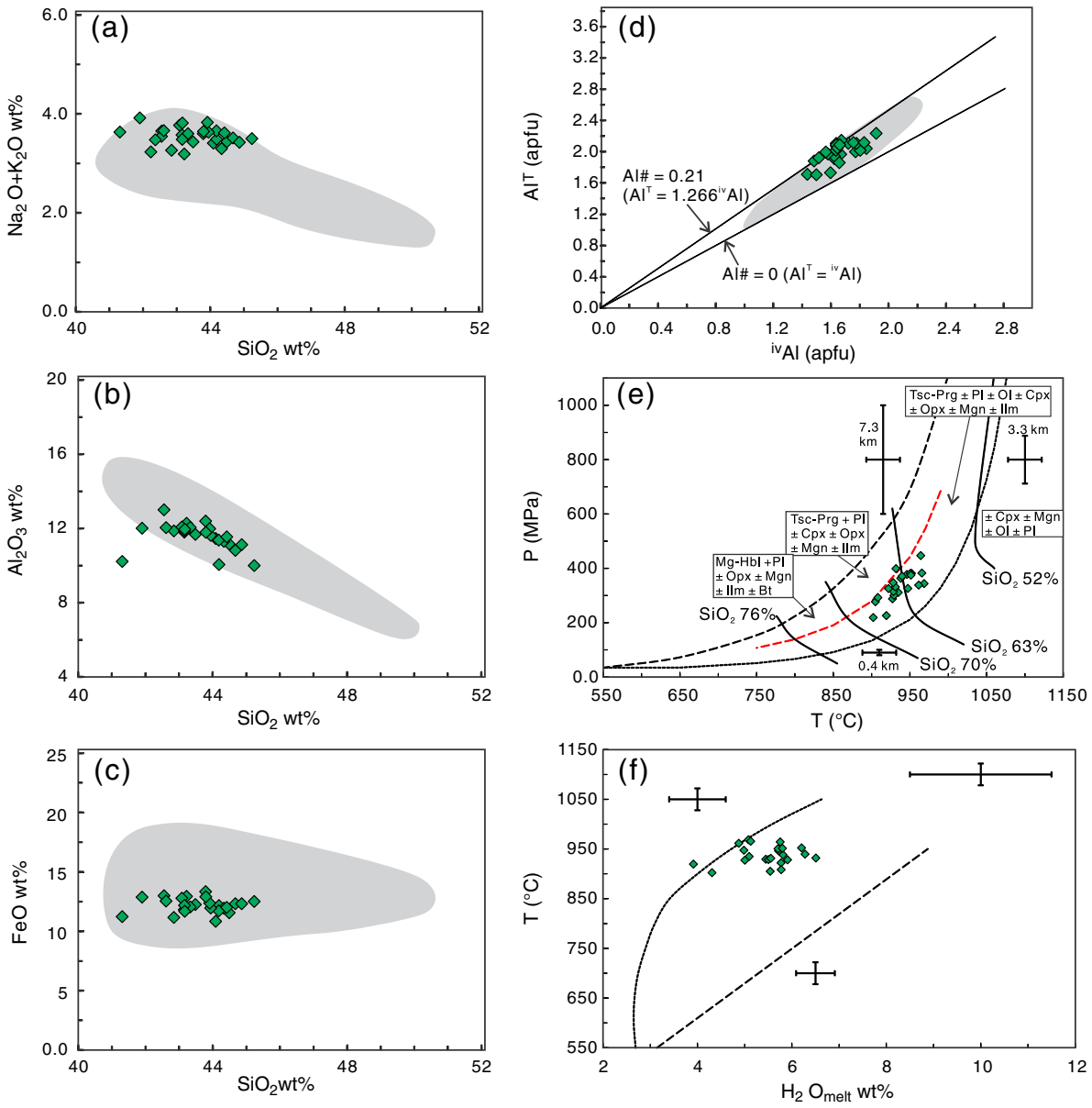

Fig. 10. Compositional variations of amphiboles. (a) Total alkali ($Na_2O + K_2O$) vs. SiO_2, (b) Al_2O_3 vs. SiO_2, (c) FeO^t vs. SiO_2, (d) Al^T vs. ^{iv}Al diagrams for amphiboles in the Xiaoling lavas. Grzy areas in (a) to (d) represent the field of volcanic amphiboles defined by Ridolfi et al. (2010). (e) P–T and (f) T–H_2O_{melt} diagrams of the analyzed amphiboles as determined by amphibole thermobarometer of Redolfi et al. (2010).

mainly evolved through fractional crystallization processes. The geochemical and mineralogical signatures of the less-contaminated samples (FS-5, 24 and 48 with MgO >6 wt.%) may reflect the nature of their mantle sources.

5.3. Evidence for a pyroxenite source

5.3.1. Constraints from bulk-rock major and trace element compositions

The follow lines of evidence suggest a pyroxenitic source for the Xiaoling lavas. First, with the exception of TiO_2, the Xiaoling lavas have major element compositions comparable to those of experimentally determined partial melts of volatile-free Mid-Ocean-Ridge Basalt (MORB)-like eclogite at 3–5 GPa (Fig. 5; e.g., Pertermann and Hirschmann, 2003; Spandler et al., 2008; Wang et al., 2014), but different from typical anhydrous peridotite-derived melts, such as MORB. The deficiency of TiO_2 in the Xiaoling samples may be attributed to the presence of Ti-oxides (e.g., rutile) in source region (Wang et al., 2014). It should be pointed out that two samples with highest SiO_2 contents (>62 wt.%) display higher Al_2O_3 contents than those of partial melts of eclogite (Fig. 5), likely because of the existence of Al-rich minerals in source region. Similarly, for a given SiO_2 content, the P_2O_5 and K_2O contents in some samples are higher than those of partial melts of eclogite at 3–5 GPa (Fig. 5), which may due to the presence of apatite and K-rich minerals (e.g., amphibole), respectively in source region. Nevertheless, many samples have comparable Al_2O_3, P_2O_5 and K_2O contents with those of partial melts of eclogite (Fig. 5). Second, the Xiaoling lavas exhibit low CaO contents (1.8–10 wt.%; Table A2; Fig. 5) that are typical of pyroxenite-derived melts, but are deficient relative to those of peridotite-derived basalts (such as MORB, 8–14 wt.%; Herzberg, 2006, 2011; Wang et al., 2014). Herzberg (2011) suggested that the bulk distribution coefficients for CaO ($D_{CaO}^{Solid/Liquid}$) of SiO_2-rich pyroxenite are generally >1, and thus low-degree melts of such source are generally low in CaO due to the dominant effects of residual clinopyroxene, whereas low-degree melts of peridotite are always enriched in CaO as its $D_{CaO}^{Solid/Liquid}$ <1. Lastly, the Xiaoling lavas have higher FeO/MnO ratios (62–91; Fe^{2+}/Fe^{total} = 0.9; e.g., Table A2) than those of partial melts of peridotite (50–60;

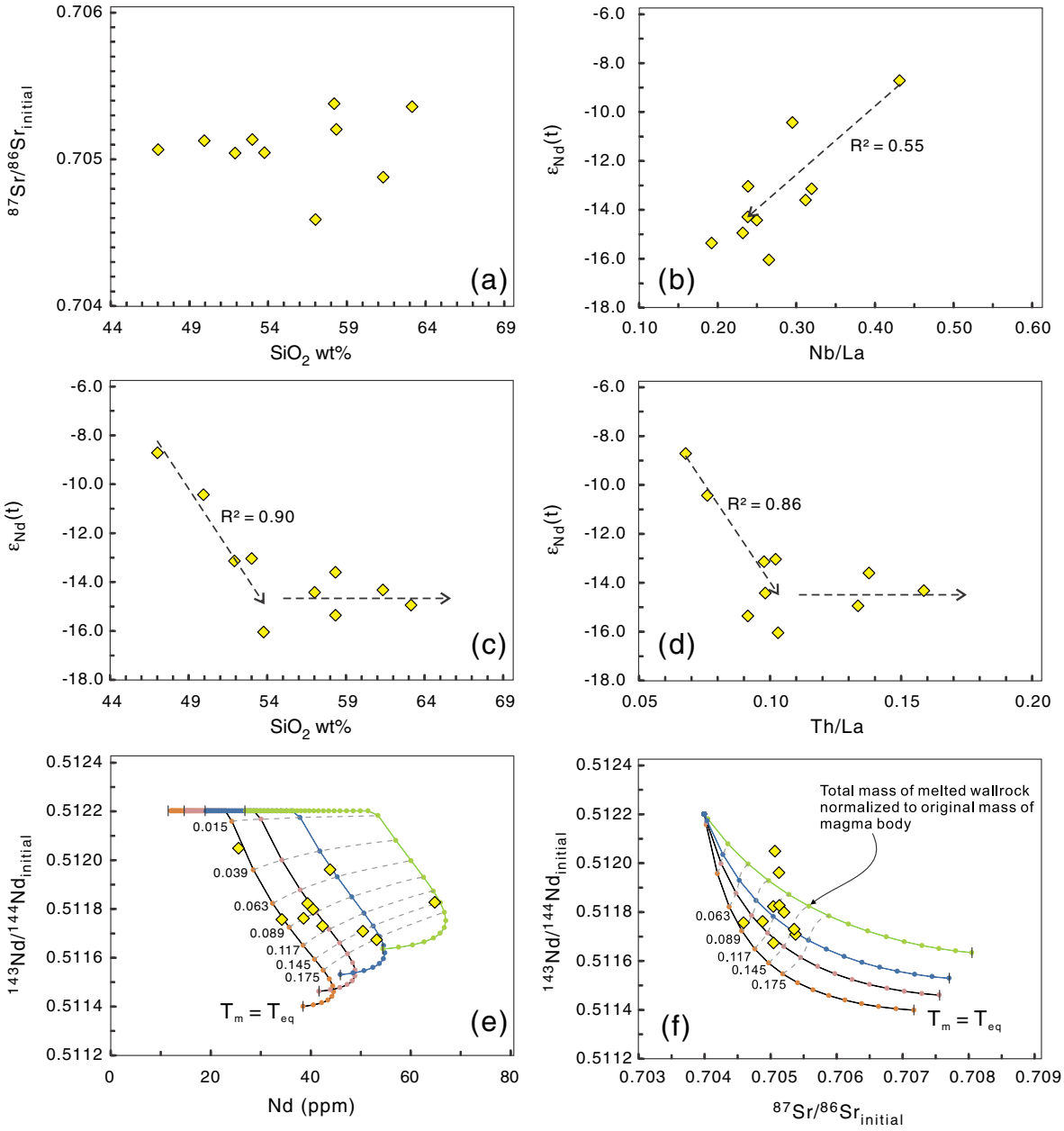

Fig. 11. Diagrams for assimilation–fractionation–crystallization discrimination (AFC) and energy-constrained AFC (EC-AFC). (a) SiO_2 vs. $^{87}Sr/^{86}Sr_{initial}$ ratios. (b) $\varepsilon_{Nd}(t)$ vs. Nb/La. (c) $\varepsilon_{Nd}(t)$ vs. SiO_2. (d) $\varepsilon_{Nd}(t)$ vs. Th/La. EC-AFC modeling for (e) initial $^{143}Nd/^{144}Nd$ vs. Nd, and (f) initial $^{143}Nd/^{144}Nd$ vs. $^{87}Sr/^{86}Sr$. Modeling parameters are listed in Table 2.

Herzberg, 2011), but comparable to those in partial melts of pyroxenite (typically >80; Herzberg, 2011). Because $D_{Mn}^{Gt/L}$ is high (2–7; Pertermann and Hirschmann, 2003), partial melts of pyroxenite are low in MnO contents when the amount of residual garnet is high (Herzberg, 2011 and references therein). Thus, the high FeO/MnO ratios of the Xiaoling lavas can be explained by the appearance of garnet in the residuum.

Niobium (Nb) concentrations can be served as an index of the degree of partial melting (Frey et al., 2000; Wang et al., 2012, 2014). Its relationship with highly incompatible trace element ratios have been used to evaluate the residual source mineralogy after stripping off the influence of the crustal contamination, the post-magmatic alteration and the fractional crystallization processes (Wang et al., 2012). Positive correlation of Tb/Yb-Nb in less-evolved samples (Fig. 12a) requires bulk solid/melt $D_{Tb/Yb}$ <1. Experimental results suggest that $D_{Tb/Yb}$ ratios for clinopyroxene/melt, amphibole/melt and phlogopite/melt partitioning are near unity, whereas $D_{Tb/Yb}$ = 0.23 for garnet/melt partitioning (Adam and Green, 2006; Dalpe and Baker, 2000; Latourrette et al., 1995; Wang et al., 2012). Thus, the positive correlation between Tb/Yb and Nb for these samples also implies the presence of residual garnet. Furthermore, negative correlations between Gd/Yb, Hf/Yb and Lu/Hf in less-evolved samples are consistent with partial melting mainly occurred in the garnet stability field (>85 km; not shown; Wang et al., 2008, 2012). It is suggested that $D_{Sc/V}$ ratios for garnet/melt, clinopyroxene/melt and amphibole/melt are nearly unity (Wang et al., 2012 and references therein). The nearly constant Sc/V ratios in less-evolved samples (Fig. 12b) imply that clinopyroxene and amphibole may be major phases in the residual mineral assemblage. It is suggested that melts equilibrium with phlogopite are expected to have significant higher Rb/Sr and lower Ba/Rb ratios, whereas melts formed from amphibole-bearing sources have lower Rb/Sr and higher Ba/Rb values (Furman and Graham, 1999). Comparing with primitive mantle, most samples are characterized by low Rb/Sr (0.01–0.05) and high Ba/Rb (19–40.3) ratios, consistent with melting of an amphibole-bearing source (Fig. 12c; Furman and Graham, 1999).

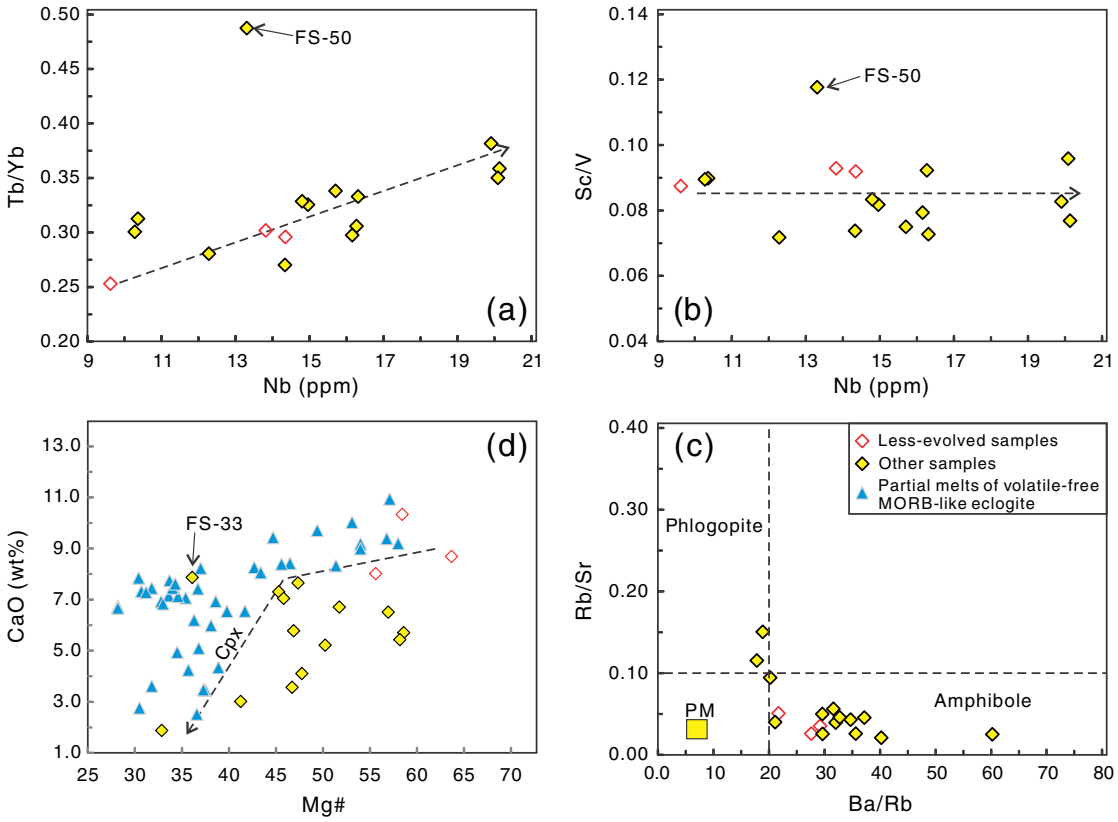

Fig. 12. Variations in incompatible trace element ratios and major element contents constrain source minerals. (a–b) Variations of trace element ratio (Tb/Yb and Sc/V) as a function of partial melting degree (Nb) in the Xiaoling lavas. (c) Rb/Sr vs. Ba/Rb (after Furman and Graham, 1999). Data sources: Primitive mantle (PM, Sun and McDonough, 1989). (d) Whole-rock CaO contents vs. Mg# diagram. Partial melts of volatile-free MORB-like eclogite at 3–5 GPa were cited from Pertermann and Hirschmann (2003) and Spandler et al. (2008).

Therefore, an amphibole-bearing garnet pyroxenite source could be a reasonable candidate to produce primary magma of the Xiaoling lavas. Further evidence for pyroxenite-dominant source is provided by olivine compositions as discussed below.

5.3.2. Constraints from olivine chemistry

As probes of parental melts, olivine phenocrysts' compositions, such as nickel (Ni), manganese (Mn), calcium (Ca) and magnesium (Mg) concentrations have been used to quantify the contributions of pyroxenite melting (Herzberg, 2011; Sobolev et al., 2005, 2007).

It has been suggested that high-Ni olivine phenocrysts in Hawaii shield-building lavas are indicative of a pyroxenite-dominated source (Herzberg, 2006, 2011; Sobolev et al., 2005, 2007). However, others argued that high-Ni olivine phenocrysts can crystallize from peridotite–melts depending on the thickness of lithosphere (Niu et al., 2011), or the crystallization temperature (Li and Ripley, 2010; Putirka et al., 2011), or the Ni content of peridotite source and its $D_{Ni}^{olivine/melt}$ (Putirka et al., 2011; Rhodes et al., 2012). Nevertheless, the essential observation is that olivines that crystallize from pyroxenite-derived melts have higher Ni contents than those from melts of peridotite-source (Herzberg, 2011).

According to Herzberg (2011), during the recycling of oceanic crust, if the bulk basaltic oceanic crust remains isolated from the surrounding peridotite, it will transform to quartz or coesite eclogite in the upper mantle and form a stage 1 pyroxenite, whereas the solid-state reaction between silica-rich recycled crust and the host peridotite will produce a second-stage (stage 2) pyroxenite. As shown in Fig. 13, olivines from samples FS-24 and FS-48 have unusually higher Ni than those of partial melts of a normal peridotite source. Moreover, olivines with Fo = 87.3 have >5000 ppm Ni contents (Fig. 13a), implying that they are unlikely to be crystallized from peridotite-derived melts (e.g., Herzberg, 2011). Such olivines can be used to calculate the composition of primary magma. The calculation reveals that primary magma may have a composition of 0.055 wt.% NiO, 9.6 wt.% MgO and 8.46 wt.% FeO^t, given a $Fe^{2+}/Fe^{total} = 0.9$, and a Fe–Mg exchange partition coefficient between olivine and basaltic liquid of 0.3 (Fig. 13a). At a given Fo, the analyzed olivines show higher Ni contents than those of olivines in the Koolau lavas from Hawaii (Fig. 13a; Herzberg, 2011; Sobolev et al., 2005, 2007). The Koolau lavas have been interpreted to be the melts derived from the stage 2 pyroxenite source (Herzberg, 2011).

The bimodal feature of Fo values between 87.3 and 80 in olivines (Fig. 8) implies that the pyroxenite source might produce melts with large range of equilibrated Fo values (Herzberg, 2011). It is shown that Ni contents decrease rapidly from 6100 to 1700 ppm for Fo >80 (corresponding to Mg# = 55 in liquid), whereas for Fo <80, Ni contents decrease slowly from 2800 to 800 ppm with decreasing Fo (Fig. 13a). Such a turning point implies that at Mg# ≥50, olivine is dominant phase in fractional mineral assemblage, whereas at Mg# <50, clinopyroxene is the dominant phase due to its low $D_{Ni}^{clinopyroxene/melt}$. Fractional crystallization of clinopyroxene will quickly deplete CaO contents in residual liquid (Wang et al., 2012). This is consistent with the turning point at Mg# ≈ 50 on Mg#–CaO trend (Fig. 12d), where the maximum CaO content is nearly constant when Mg#>50, but decreases rapidly from ~7.6 wt.% at Mg# = 48 to ~2.0 wt.% at Mg# = 33, with the exception of that from sample FS-33.

In addition, the analyzed olivines have identical Ca contents with olivines derived from the Koolau lavas at a given Fo value, but lower than those crystallized from peridotite-derived melts (Fig. 13b). Low Ca contents in the analyzed olivines are consistent with the low whole-rock CaO contents discussed above, suggesting a pyroxenite-dominant source (Herzberg, 2011; Sobolev et al., 2007). Analyzed olivines mostly (>85% of total analyses) have lower Mn contents and higher Fe/Mn ratios than those of peridotite melts and their derivative liquids (Fig. 13c–d), also suggesting the importance of garnet pyroxenite in the source (e.g., Herzberg, 2011; Liu et al., 2008; Sobolev et al., 2005, 2007).

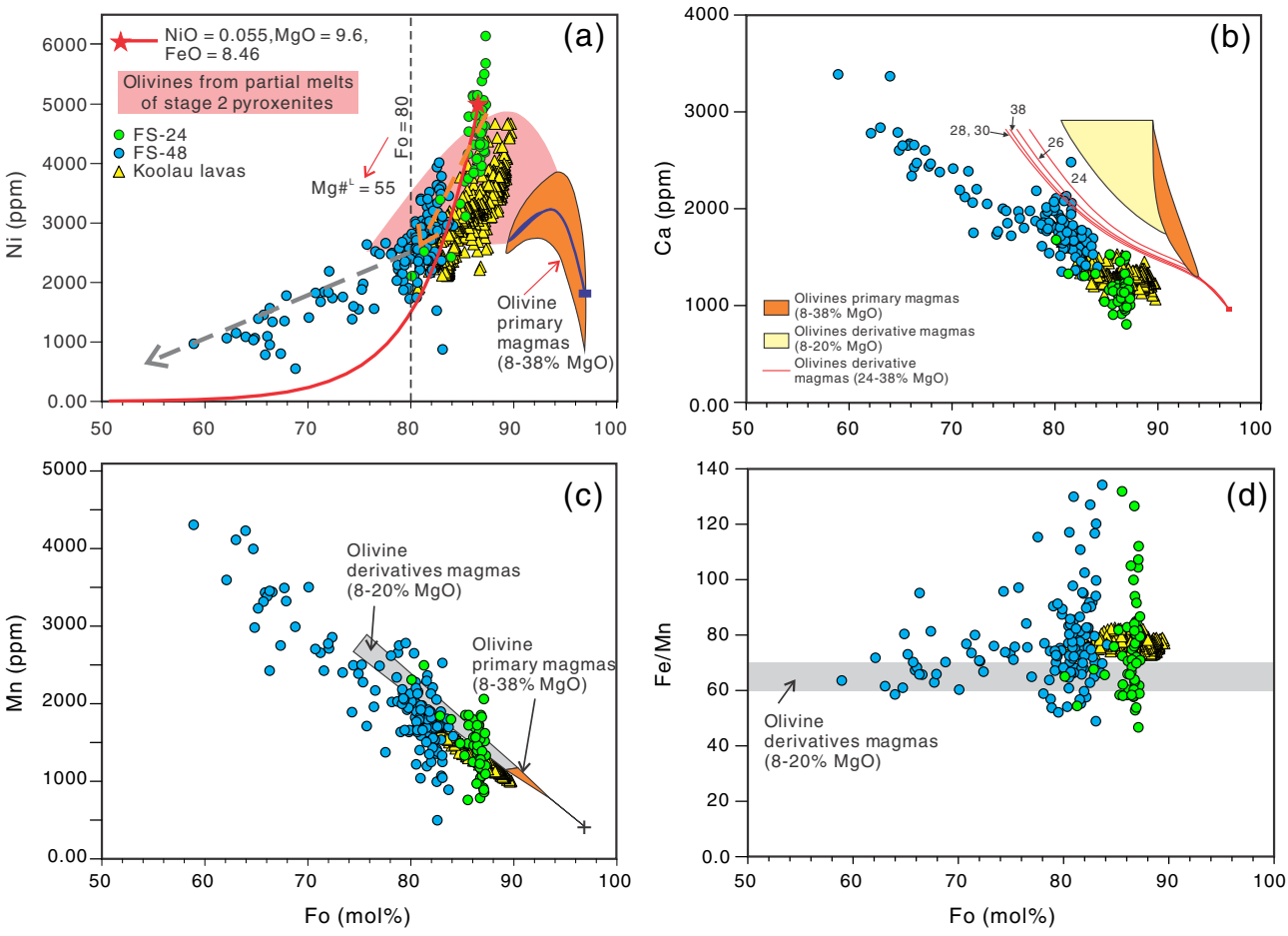

Fig. 13. Calculated olivine phenocryst compositions for melts of a peridotite source compared with olivines from Koolau and Xiaoling lavas. (a) High Ni concentrations and variable Fo values for the Xiaoling olivines are similar to those of olivines crystallized from pyroxenite source. (b) Low Ca concentrations in olivine reflects the low Ca contents in the Xiaoling lavas. Most Xiaoling olivines are (c) lower in Mn concentrations, but (d) higher in Fe/Mn ratios than those from peridotite sources. Data of the Koolau lavas are from Sobolev et al. (2007), while the discrimination diagrams for pyroxenite are after Herzberg (2011).

5.4. Evidence for multiple mantle metasomatic events

Parental melts of pyroxenites are frequently considered as important agent of mantle metasomatism (Bodinier et al., 1990; Menzies et al., 1985). However, pyroxenites themselves may be metasomatized too (Garrido and Bodinier, 1999; Xu, 2002). The following provides a brief discussion on when and how the inferred pyroxenite source was formed, and its subsequent metasomatism by younger geological events.

Pyroxenitic xenoliths such as garnet pyroxenite, Cr–pyroxenite, Al–augite pyroxenite, and websterite are abundant in late Mesozoic to Cenozoic basalts in the NCC and adjacent areas (Liu et al., 2005; Xu, 2002; Ying et al., 2013; Yu et al., 2010; Zhang et al., 2010). Thus, pyroxenite could be an important component in the mantle underlying the NCC during the late Mesozoic to Cenozoic. For instance, Hong et al. (2013) showed that the late Cenozoic basalts in the northern margin of the NCC may have been derived from a pyroxenite source. These basalts have positive $\varepsilon_{Nd}(t)$ values, implying that the pyroxenites may exist in the asthenospheric mantle or is newly formed within the SCLM (Hong et al., 2013). In contrast to the Cenozoic basalts in the NCC, the Xiaoling lavas have arc-like trace element distribution patterns (enrichment of LILE and depletion of HFSE) and EM1-like Sr–Nd isotopic compositions, resembling those of the Early Cretaceous Luxi mafic rocks in the NCC (Fig. 7; Guo et al., 2003; Huang et al., 2012). These are typical characteristics of the Mesozoic SCLM beneath the interior of the NCC, which was generally attributed to metasomatized events (Guo et al., 2003; Huang et al., 2012).

Arc-like trace element distribution patterns and enriched Sr–Nd isotopic signatures of the Cretaceous mafic rocks in the southeastern NCC were interpreted to be originated from the SCLM metasomatized by melts/fluids of the subducted Yangtze lithosphere during the Triassic collision between the NCC and the Yangtze plate (Fan et al., 2001; Jahn, et al., 1999; Yang et al., 2012a; Ying et al., 2013; Zhang et al., 2002). The key evidence for the linkage between the metasomatism and Triassic continental subduction is from the ca. 125 Ma Fangcheng basalts (Zhang et al., 2002) and Yinan gabbros (Xu et al., 2004). These mafic rocks are generally characterized by EM2-like isotopic signatures with relatively high initial $^{87}Sr/^{86}Sr$ ratios (>0.708) and low $\varepsilon_{Nd}(t)$ values (Fig. 7; Xu et al., 2004; Zhang et al., 2002; Zhao et al., 2013). However, the Xiaoling lavas show low initial Sr isotopes and $\varepsilon_{Nd}(t)$ values, which significantly differ from those of the Fangcheng and Yinan mafic rocks (Fig. 7). Furthermore, the 130 Ma Liaodong–Jinan mafic intrusive rocks have relatively lower initial $^{206}Pb/^{204}Pb$ (15.13–17.85), $^{207}Pb/^{204}Pb$ (15.02–15.58) and $^{208}Pb/^{204}Pb$ (35.39–38.54) ratios than the respective ratios of the subducted Yangtze lithosphere ($^{206}Pb/^{204}Pb$ = 17.957–18.620, $^{207}Pb/^{204}Pb$ = 15.508–15.655, $^{208}Pb/^{204}Pb$ = 38.129–38.710) (Pei et al., 2011; Yang et al., 2008a). It is suggested that the spatial extent of the NCC influenced by the subducted Yangtze lithosphere is less than 200 km away from the Dabie–Sulu orogenic belt (Yang et al., 2012a). The predominance of negative ε_{Nd} coesite-bearing eclogites in the Dabie–Sulu terrane also does not support the existence of large-scale oceanic crust prior to the collision between the NCC and the Yangtze plate (Fan et al., 2001).

However, Cretaceous mafic magmatism with similar trace element and isotopic compositions is widespread in the NCC, distributing extensively in the Taihangshan region and the western Shandong and Liaoning provinces (Chen and Zhai, 2003; Guo et al., 2001; Huang et al., 2012; Yang and Li, 2008; Yang et al., 2004a). All these suggest that the subducted Yangtze plate did not play a dominant role in forming EM1-like mantle reservoir of the Xiaoling lavas.

Except for the Yangtze plate, the NCC was subducted by the Paleo-Asian oceanic plate to the north during the Paleozoic to the Triassic, and the Pacific plate to the east during the Jurassic to the Cretaceous (Windley et al., 2010). The initial SCLM could also have been modified by these subduction processes (Windley et al., 2010; Xu et al., 2009; Zheng and Wu, 2009; Zhu et al., 2012b). It should be pointed out that the subducted Paleo-Asian oceanic crust in the north of the NCC may also release fluid content to metasomatize and hydrate the NCC (e.g., Windley et al., 2010). According to the field geology and geochronology, Xu et al. (2013) proposed that the subduction of the Paleo-Asian oceanic crust and subsequent collision between the NCC and Mongolia microcontinents accomplished by ca. 380 Ma, which is much earlier than the timing of the peak magmatism corresponding to the destruction of the NCC. Although the subduction of the Paleo-Asian oceanic plate could have initialized the destruction of the northern NCC, it may not be the major force for the continental-scale replacement of the SCLM of the NCC (Xu et al., 2009). Nevertheless, the current available data cannot demonstrate the role of the subducted Paleo-Asian oceanic crust in metasomatism and hydration of the mantle source for the Xiaoling lavas.

Recent studies identified that the recycled Pacific oceanic crust can contribute to late Mesozoic to Cenozoic magma source as components with various $^{87}Sr/^{86}Sr$ ratios (<0.7030–>0.7065) and positive ε_{Nd} values (+2–+8) (Xu, 2014; Xu et al., 2012). The EM1-like signatures of the Xiaoling lavas therefore rule out significant contribution of partial melts of the subducted Pacific oceanic crust. Furthermore, the negative $\varepsilon_{Nd}(t)$ values of the Xiaoling lavas suggest a long-term isolated and low Sm/Nd source. Therefore, we favor a large-scale and long-lasting subduction-induced metasomatic event in the Late Archean to Paleoproterozoic to account for the geochemical and isotopic features of the pyroxenite source of the Xiaoling lavas (e.g., Yang et al., 2004a). Subduction process might have been prevalent around the Eastern Block of the NCC between 1.95 and 2.5 Ga as recorded by arc-related igneous rocks (Faure et al., 2004; Peng et al., 2013; Polat et al., 2006). Recycled crustal materials could have directly transformed into the stage 1 pyroxenite, or they could have reacted with surrounding mantle peridotite in solid-state to generate the stage 2 pyroxenite (Herzberg, 2011). Partial melting of the stage 2 pyroxenite can produce the high-Ni olivines in the Xiaoling lavas (Fig. 13a). In addition, Huang et al. (2012) postulated that addition (1 to 4 wt.%; Fig. 7) of recycled crustal materials to the asthenospheric mantle at ca. 2.1 Ga can explain the formation of the EM1-like SCLM. The above considerations lead us to suggest that the pyroxenite source for the Xiaoling lavas could have been formed during the Late Archean–Palaeoproterozoic metasomatic events. This Late Archean–Paleoproterozoic pyroxenitic mantle source in turn may have been metasomatized by fluids released from the subducted Pacific slab as discussed below.

The low initial $^{87}Sr/^{86}Sr$ ratios (0.7046–0.7054) and highly negative ε_{Nd} values (−8.7–−16) (Table 1) suggest that the Xiaoling lavas were derived from a long-term isolated mantle source with low Rb/Sr and Sm/Nd ratios. However, the Xiaoling lavas have high Rb/Sr ratios (0.02–0.12) and display positive Rb anomalies in Fig. 6. Because Rb (as well as other LILE) is a fluid-mobile element (e.g., Berly et al., 2006), the coexistence of low initial Sr isotopes and high Rb/Sr ratios then implies a recent addition of fluid-enriched components for the enrichment of LILE in the source of the Xiaoling lavas. Such a LILE enrichment of the Mesozoic SCLM may occur during or shortly prior to the melting event (Guo et al., 2003).

The high water contents (Xia et al., 2013) and arc-like geochemical signatures (Fan et al., 2001; Guo et al., 2001, 2003; Huang et al., 2012; Pei et al., 2011) are common feature of Mesozoic melts derived from the SCLM. The fractional crystallization experimental studies showed that amphibole is present only at water-saturated conditions and relatively low liquidus temperatures (Berndt et al., 2005; Botcharnikov et al., 2008). Thus, the presence of abundant amphibole phenocrysts in the Xiaoling lavas strongly suggests a hydrous parental magma. The chemical compositions of the igneous amphibole can be used to calculate the liquidus temperature and melt water contents (e.g., Ridolfi et al., 2010). As shown in Fig. 10, the amphibole chemical compositions of the Xiaoling lavas suggest a high melt water contents (up to 6.5%) for their parental magmas. This implies that the mantle source of the Xiaoling lavas should be highly hydrated. This highly hydrated SCLM cannot be long-term stable because the addition of water to the SCLM will significantly decrease its viscosity (Karato, 2010; Peslier et al., 2010). Therefore, we propose another younger metasomatic event that imparted the enrichment of LILE, and large amount of water (and possible other fluid phases) to the SCLM. This young metasomatism is most likely related to fluids released from the Pacific slab, which could have hydrated the SCLM beneath the studied area, and triggered the instability of the NCC, as suggested by Windley et al. (2010). Additional supporting evidences for the relationship with the Pacific subduction include: (1) Zhu et al. (2012a) showed that the principal extension directions in the eastern NCC varied synchronously with the subduction direction of the Pacific plate (and the Izanagi plate) during the Cretaceous to Paleogene; (2) The Cretaceous giant igneous event and large-scale lode gold (Au) mineralization in eastern China occurred coincidently with an abrupt change in drifting direction of the subducted Pacific plate (Sun et al., 2007).

5.5. Implication for lithospheric thinning

The primary geochemical and isotopic compositions of mafic rocks serve as rock probe to detect the thermochemical state of deep Earth's mantle (Herzberg et al., 2007; Putirka, 2005; Wang et al., 2008, 2009, 2012, 2013, 2014), which are crucial to understand the destruction of the NCC. The destruction of the NCC was suggested to initiate as early as the Late Carboniferous along its northern margin (Xu et al., 2009; Zhu et al., 2012b), but commenced during the Late Triassic along its eastern/northeastern margin as recorded by the 224–210 Ma mafic/felsic intrusions in the Liaodong and Jiaodong Peninsulas and the ca. 223 Ma kimberlites from North Korea (Yang et al., 2005, 2007b, 2010, 2012b). Geochemically, the 224–210 Ma mafic intrusions (including diorite, shoshonitic and tholeiitic dolerite) in the Liaodong Peninsula can be divided into two sub-types. One has variable initial $^{87}Sr/^{86}Sr$ ratios (0.7049–0.7153), $\varepsilon_{Nd}(t)$ (−14.5–+0.4) and $\varepsilon_{Hf}(t)$ values (−10–+6.2), whereas the other shows low initial $^{87}Sr/^{86}Sr$ ratios (0.7049–0.7074), $\varepsilon_{Nd}(t)$ (−13.4–−7.6) and $\varepsilon_{Hf}(t)$ values (−14–−5.6) (Fig. 14; Yang et al., 2007b, 2012b). This implies that the Late Triassic SCLM beneath the Liaodong Peninsula was likely characterized by the coexistence of the juvenile and ancient lithospheric mantle (Yang et al., 2007b, 2010, 2012b). It thus had been suggested that the ancient cratonic lithospheric mantle had been removed and replaced by juvenile (fertile) lithospheric mantle ("decratonization") at ca. 210 Ma due to the lithospheric delamination in the Liaodong Peninsula (Yang et al., 2007b, 2010). The delamination of the lithospheric mantle was caused by facies transformation of lower crustal mafic paragneisis to eclogite or garnet clinopyroxenite during the collision between the NCC and the Yangtze plate (Yang et al., 2007b).

However, the absence of the Late Triassic basaltic–andesitic rocks in the Liaodong Peninsula implies that the extent of the delaminated lithospheric mantle (and/or crust) may be small. Therefore their ability to sink was limited, and the corresponding ascending asthenospheric column was short and unlikely melted extensively (Ducea, 2011). Because of its higher density, the delaminated ancient lithospheric mantle

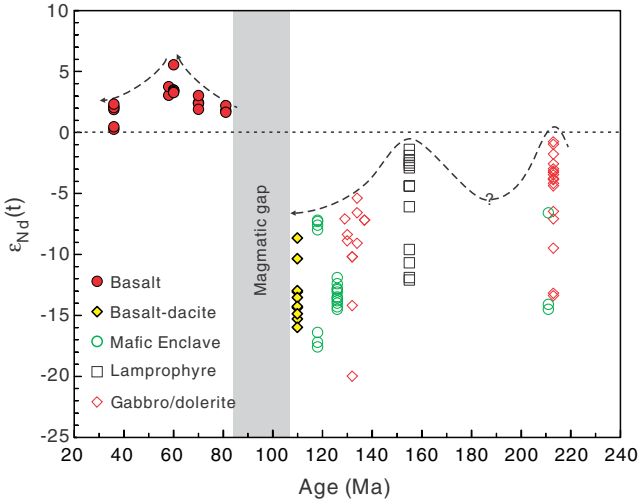

Fig. 14. A plot of age vs. $\varepsilon_{Nd}(t)$ values for the Late Triassic to Eocene mafic rocks in the Liaodong Peninsula. Data sources: 220–210 Ma mafic intrusions and enclaves (Yang et al., 2007a,b, 2012b); 155 Ma Huaziyu lamprophyres (Jiang et al., 2010); 130 Ma mafic intrusions (Pei et al., 2011); 126–120 Ma mafic enclaves (Yang et al., 2004b); 80–36 Ma basalts (Kuang et al., 2012; Wang et al., 2006, 2007).

(i.e., eclogite/garnet pyroxenites) cannot be preserved in the asthenospheric mantle for a long term. If correct, it could not be a dominant source of the Jurassic and Cretaceous magmatism. This is supported by the preservation of isotope-enriched mantle signatures sampled by the 155 Ma Huaziyu lamprophyres (ε_{Nd}(155 Ma) = −12.1–−1.4, $^{87}Sr/^{86}Sr_{(155\ Ma)}$ = 0.7073–0.7117; Jiang et al., 2005), the 130 Ma mafic intrusions (ε_{Nd}(130 Ma) = −20–−5.4, $^{87}Sr/^{86}Sr_{(130\ Ma)}$ = 0.7056–0.7119; Pei et al., 2011), and the 110 Ma Xiaoling lavas in the Liaodong Peninsula (ε_{Nd}(110 Ma) = −16–−8.7, $^{87}Sr/^{86}Sr_{(110\ Ma)}$ = 0.7046–0.7055; Figs. 7, 14; Table 1).

The Huaziyu lamprophyre is the only identified case of mafic magmatism in the Liaodong Peninsula during the Jurassic. Their whole-rock $\varepsilon_{Nd}(t)$ values of −12.1–−1.4 were interpreted to be indicative of a derivations from an enriched lithospheric mantle with the involvement of asthenospheric mantle components (Jiang et al., 2005, 2010). Recent studies on the Early Cretaceous granitic rocks in this region revealed that a felsic dike of 125 Ma has positive whole-rock $\varepsilon_{Nd}(t)$ and $\varepsilon_{Hf}(t)$ values of +4.7 and +9.3, respectively, implying a stronger asthenospheric signature in the Cretaceous magmas (Yang et al., 2008b). The subsequent asthenosphere-derived basalts were not formed until 80 Ma in the Liaodong Peninsula (Fig. 14; Kuang et al., 2012; Liu et al., 1993; Wang et al., 2006, 2007). It seems that increasing asthenosphere-derived magmas were involved in the Mesozoic magmatism with time in the Liaodong Peninsula, likely corresponding to a progression from local to dominant upwelling of the asthenosphere. All these information collectively suggest that in the NCC the complete replacement of cratonic SCLM by young, juvenile lithospheric mantle only accomplished after the late Cretaceous (Xu, 2001). In the Liaodong case, the lithospheric thinning encompasses at least 75 Ma (from 155 to 80 Ma). Such a prolonged lithospheric thinning and replacement process is consistent with the thermo-mechanical erosion caused by laterally convective asthenosphere (Xu, 2001).

6. Conclusions

(i). The Xiaoling lavas, consisting of basalt, andesite and dacite, were erupted at ca. 110 Ma in the Liaodong Peninsula, following the magmatic climax during the destruction of the NCC. They have a wide range of SiO_2 (45–62 wt.%), MgO (1.2–9.2 wt.%) and CaO (1.8–10 wt.%) contents, and are characterized by LILE enrichment and HFSE depletion, and EM1-like Sr–Nd isotopes.

(ii). The Xiaoling lavas with relatively high-SiO_2 (>54 wt.%) contents underwent insignificant crustal contamination during magma ascending, whereas the low-SiO_2 samples (<54 wt.%) were contaminated by ancient, felsic lower crustal materials of the NCC. The estimated involvement ratios of lower crustal materials in magma body vary between 0.015 and 0.175. The least contaminated samples are characterized by high-MgO (>6 wt.%) and low-SiO_2 contents, and abundance of olivine phenocrysts.

(iii). Major element compositions of the Xiaoling lavas are similar to those of partial melts of volatile-free MORB-like eclogite at 3–5 GPa, but differ significantly from typical anhydrous peridotite-derived melts. High Ni and Fe/Mn, and low Ca contents in olivine phenocrysts are consistent with crystallization from partial melts of a garnet pyroxenite mantle source.

(iv). The pyroxenite mantle source of the Xiaoling lavas may have been formed during the Archean–Palaeoproterozoic metasomatic events, through the solid-state reaction between recycled crustal materials and surrounding peridotite. This source was further metasomatized by fluids from the subducted Pacific plate during the late Mesozoic. Invasion of high water contents to the SCLM may have considerably decreased its strength and triggered the destruction of the NCC.

Acknowledgments

This paper reports part of a PhD study by CJ Pang. We are grateful to Editor Sun-Lin Chung and three anonymous reviewers for their constructive suggestions and comments that improved the quality of the manuscript. We thank Y Liu, XL Tu, XR Liang, HN Qiu, GQ Wang, J Li, XY Jiang, LF Xie and HY Chen for technical assistance with diverse analyses. We thank XL Huang and TP Peng for helpful discussion. This study is jointly supported by the Natural Science Foundation of China (91014007; 40914001), the CAS/SAFEA International Partnership Program for Creative Research Teams (KZCX2-YW-Q04-06), and the Australian Research Council (ARC) Future Fellowship (FT140100826) for Xuan-Ce Wang. This study is also supported by the research grant of State Key Laboratory of Isotope Geochemistry, Guangzhou Institute of Geochemistry, Chinese Academy of Sciences (SKLIG-KF-13-07, SKLIG-KF-14-06). This is GIGCAS Publication No. 2058.

Appendix A. Supplementary data

Supplementary data to this article can be found online at http://dx.doi.org/10.1016/j.lithos.2015.03.022.

References

Adam, J., Green, T., 2006. Trace element partitioning between mica- and amphibole-bearing garnet lherzolite and hydrous basanitic melt: 1 Experimental results and the investigation of controls on partitioning behaviour. Contributions to Mineralogy and Petrology 152, 1–17.

Berly, T.J., Hermann, J., Arculus, R.J., Lapierre, H., 2006. Supra-subduction zone pyroxenites from San Jorge and Santa Isabel (Solomon Islands). Journal of Petrology 47, 1531–1555.

Berndt, J., Koepke, J., Holtz, F., 2005. An experimental investigation of the influence of water and oxygen fugacity on differentiation of MORB at 200 MPa. Journal of Petrology 46, 135–167.

BGMR, 1989. Regional Geology of Liaoning Province, People's Republic of China (in Chinese with English abstract). Geological Publishing House, Beijing.

Bodinier, J.L., Vasseur, G., Vernieres, J., Dupuy, C., Fabries, J., 1990. Mechanisms of mantle metasomatism: geochemical evidence from the lherz orogenic peridotite. Journal of Petrology 31, 597–628.

Bohrson, W.A., Spera, F.J., 2001. Energy-constrained open-system magmatic processes II: Application of energy-constrained assimilation-fractional crystallization (EC-AFC) model to magmatic systems. Journal of Petrology 42, 1019–1041.

Botcharnikov, R.E., Almeev, R.R., Koepke, J., Holtz, F., 2008. Phase relations and liquid lines of descent in hydrous ferrobasalt—implications for the Skaergaard intrusion and Columbia River flood basalts. Journal of Petrology 49, 1687–1727.

Chen, B., Zhai, M., 2003. Geochemistry of late Mesozoic lamprophyre dykes from the Taihang Mountains, north China, and implications for the sub-continental lithospheric mantle. Geological Magazine 140, 87–93.

Dalpe, C., Baker, D.R., 2000. Experimental investigation of large-ion-lithophile-element-, high-field-strength-element- and rare-earth-element-partitioning between calcic amphibole and basaltic melt: the effects of pressure and oxygen fugacity. Contributions to Mineralogy and Petrology 140, 233–250.
DePaolo, D.J., 1981. Trace element and isotopic effects of combined wallrock assimilation and fractional crystallization. Earth and Planetary Science Letters 53, 189–202.
DePaolo, D.J., Daley, E.E., 2000. Neodymium isotopes in basalts of the southwest basin and range and lithospheric thinning during continental extension. Chemical Geology 169, 157–185.
Ducea, M.N., 2011. Fingerprinting orogenic delamination. Geology 39, 191–192.
Fan, W.M., Zhang, H.F., Baker, J., Jarvis, K.E., Mason, P.R.D., Menzies, M.A., 2000. On and off the North China Craton: where is the Archaean Keel? Journal of Petrology 41, 933–950.
Fan, W.M., Guo, F., Wang, Y.J., Lin, G., Zhang, M., 2001. Post-orogenic bimodal volcanism along the Sulu orogenic belt in Eastern China. Physics and Chemistry of the Earth, Part A: Solid Earth and Geodesy 26, 733–746.
Faure, M., Lin, W., Monié, P., Bruguier, O., 2004. Palaeoproterozoic arc magmatism and collision in Liaodong Peninsula (north-east China). Terra Nova 16, 75–80.
Frey, F.A., Clague, D., Mahoney, J.J., Sinton, J.M., 2000. Volcanism at the edge of the Hawaiian plume: petrogenesis of submarine alkalic lavas from the North Arch volcanic field. Journal of Petrology 41, 667–691.
Furman, T., Graham, D., 1999. Erosion of lithospheric mantle beneath the East African Rift system: geochemical evidence from the Kivu volcanic province. Lithos 48, 237–262.
Gao, S., Rudnick, R.L., Carlson, R.W., McDonough, W.F., Liu, Y.-S., 2002. Re–Os evidence for replacement of ancient mantle lithosphere beneath the North China craton. Earth and Planetary Science Letters 198, 307–322.
Gao, S., Rudnick, R.L., Yuan, H.L., Liu, X.M., Liu, Y.S., Xu, W.L., Ling, W.L., Ayers, J., Wang, X.C., Wang, Q.H., 2004. Recycling lower continental crust in the North China craton. Nature 432, 892–897.
Garrido, C.J., Bodinier, J.-L., 1999. Diversity of mafic rocks in the Ronda peridotite: evidence for pervasive melt–rock reaction during heating of subcontinental lithosphere by upwelling asthenosphere. Journal of Petrology 40, 729–754.
Griffin, W.L., Zhang, A., O'Reilly, S.Y., Ryan, C.G., 1998. Phanerozoic evolution of the lithosphere beneath the Sino-Korean craton. In: Flower, M.F.J., Chung, S.-L., Lo, C.-H., Lee, T.-Y. (Eds.), Mantle Dynamics and Plate Interactions in East Asia: Geodynamics Series.American Geophysical Union, pp. 107–126
Guo, F., Fan, W.M., Wang, Y.J., Lin, G., 2001. Late mesozoic mafic intrusive complexes in North China Block: constraints on the nature of subcontinental lithospheric mantle. Physics and Chemistry of the Earth, Part A: Solid Earth and Geodesy 26, 759–771.
Guo, F., Fan, W.M., Wang, Y.J., Lin, G., 2003. Geochemistry of late mesozoic mafic magmatism in west Shandong Province, eastern China: characterizing the lost lithospheric mantle beneath the North China Block. Geochemical Journal 37, 63–77.
Herzberg, C., 2006. Petrology and thermal structure of the Hawaiian plume from Mauna Kea volcano. Nature 444, 605–609.
Herzberg, C., 2011. Identification of source lithology in the Hawaiian and Canary Islands: implications for origins. Journal of Petrology 52, 113–146.
Herzberg, C., Asimow, P.D., Arndt, N., Niu, Y., Lesher, C.M., Fitton, J.G., Cheadle, M.J., Saunders, A.D., 2007. Temperatures in ambient mantle and plumes: constraints from basalts, picrites, and komatiites. Geochemistry, Geophysics, Geosystems 8, Q02006.
Hirschmann, M.M., Stolper, E.M., 1996. A possible role for garnet pyroxenite in the origin of the "garnet signature" in MORB. Contributions to Mineralogy and Petrology 124, 185–208.
Hong, L.B., Zhang, Y.H., Qian, S.P., Liu, J.Q., Ren, Z.Y., Xu, Y.G., 2013. Constraints from melt inclusions and their host olivines on the petrogenesis of Oligocene–Early Miocene Xindian basalts, Chifeng area, North China Craton. Contributions to Mineralogy and Petrology 165, 305–326.
Huang, X.-L., Zhong, J.-W., Xu, Y.-G., 2012. Two tales of the continental lithospheric mantle prior to the destruction of the North China Craton: insights from Early Cretaceous mafic intrusions in western Shandong, East China. Geochimica Et Cosmochimica Acta 96, 193–214.
Jahn, B.-m., Wu, F., Lo, C.-H., Tsai, C.-H., 1999. Crust–mantle interaction induced by deep subduction of the continental crust: geochemical and Sr–Nd isotopic evidence from post-collisional mafic–ultramafic intrusions of the northern Dabie complex, central China. Chemical Geology 157, 119–146.
Jiang, Y., Jiang, S., Zhao, K., Ni, P., Ling, H., Liu, D., 2005. SHRIMP U–Pb zircon dating for lamprophyre from Liaodong Peninsula: constraints on the initial time of Mesozoic lithosphere thinning beneath eastern China. Chinese Science Bulletin 50, 2612–2620.
Jiang, Y.-H., Jiang, S.-Y., Ling, H.-F., Ni, P., 2010. Petrogenesis and tectonic implications of Late Jurassic shoshonitic lamprophyre dikes from the Liaodong Peninsula, NE China. Mineralogy and Petrology 100, 127–151.
Karato, S.-i., 2010. Rheology of the deep upper mantle and its implications for the preservation of the continental roots: a review. Tectonophysics 481, 82–98.
Kuang, Y.S., Wei, X., Hong, L.B., Ma, J.L., Pang, C.J., Zhong, Y.T., Zhao, J.X., Xu, Y.G., 2012. Petrogenetic evaluation of the Laohutai basalts from North China Craton: melting of a two-component source during lithospheric thinning in the late Cretaceous–early Cenozoic. Lithos 154, 68–82.
Latourrette, T., Hervig, R.L., Holloway, J.R., 1995. Trace-element partitioning between amphibole, phlogopite, and basanite melt. Earth and Planetary Science Letters 135, 13–30.
Le Bas, M.J., Maitre, R.W.L., Streckeisen, A., Zanettin, B., 1986. A chemical classification of volcanic rocks based on the total alkali–silica diagram. Journal of Petrology 27, 745–750.
Leake, B.E., Woolley, A.R., Arps, C.E.S., Birch, W.D., Gilbert, M.C., Grice, J.D., Hawthorne, F.C., Kato, A., Kisch, H.J., Krivovichev, V.G., Linthout, K., Laird, J., Mandarino, J.A., Maresch, W.V., Nickel, E.H., Rock, N.M.S., Schumacher, J.C., Smith, D.C., Stephenson, N.C.N., Ungaretti, L., Whittaker, E.J.W., Youzhi, G., 1997. Nomenclature of amphiboles; report of the subcommittee on amphiboles of the International Mineralogical Association, Commission on New Minerals and Mineral Names. The Canadian Mineralogist 35, 219–246.
Li, C.S., Ripley, E.M., 2010. The relative effects of composition and temperature on olivine-liquid Ni partitioning: statistical deconvolution and implications for petrologic modeling. Chemical Geology 275, 99–104.
Li, S.G., Xiao, Y.L., Liou, D.L., Chen, Y.Z., Ge, N.J., Zhang, Z.Q., Sun, S.S., Cong, B.L., Zhang, R.Y., Hart, S.R., Wang, S.S., 1993. Collision of the North China and Yangtse Blocks and formation of coesite-bearing eclogites—timing and processes. Chemical Geology 109, 89–111.
Liu, D.Y., Nutman, A.P., Compston, W., Wu, J.S., Shen, Q.H., 1992. Remnants of ≥3800 Ma crust in the Chinese part of the Sino-Korean craton. Geology 20, 339–342.
Liu, C., Xie, G., Wei, K., 1993. Isotope and rare element geochemistry of the Huangyishan Basalt, Kuandian, Liaoning Province, China. Acta Petrologica Sinica 9, 9–19.
Liu, Y., Gao, S., Lee, C.-T.A., Hu, S., Liu, X., Yuan, H., 2005. Melt–peridotite interactions: links between garnet pyroxenite and high-Mg# signature of continental crust. Earth and Planetary Science Letters 234, 39–57.
Liu, Y., Gao, S., Kelemen, P.B., Xu, W., 2008. Recycled crust controls contrasting source compositions of Mesozoic and Cenozoic basalts in the North China Craton. Geochimica et Cosmochimica Acta 72, 2349–2376.
Mckenzie, D., Bickle, M.J., 1988. The volume and composition of melt generated by extension of the lithosphere. Journal of Petrology 29, 625–679.
Meng, Q.R., Zhang, G.W., 1999. Timing of collision of the North and South China blocks: controversy and reconciliation. Geology 27, 123–126.
Menzies, M.A., Xu, Y., 1998. Geodynamics of the North China Craton. In: Chung, S.-L., Lo, C.-H., Lee, T.-Y. (Eds.), Flower, M.F.J.American Geophysical Union, Mantle Dynamics and Plate Interactions in East Asia, pp. 155–165
Menzies, M., Kempton, P., Dungan, M., 1985. Interaction of continental lithosphere and asthenospheric melts below the Geronimo Volcanic Field, Arizona, U.S.A. Journal of Petrology 26, 663–693.
Menzies, M.A., Fan, W., Zhang, M., 1993. Palaeozoic and Cenozoic lithoprobes and the loss of >120 km of Archaean lithosphere, Sino-Korean craton, China. Geological Society, London, Special Publications 76, 71–81.
Menzies, M., Xu, Y., Zhang, H., Fan, W., 2007. Integration of geology, geophysics and geochemistry: a key to understanding the North China Craton. Lithos 96, 1–21.
Morimoto, N., 1988. Nomenclature of pyroxenes. Mineralogy and Petrology 39, 55–76.
Niu, Y., 2005. Generation and evolution of basaltic magmas: some basic concepts and a new view on the origin of Mesozoic–Cenozoic basaltic volcanism in eastern China. Geological Journal of China Universities 11, 9–46.
Niu, Y.L., Wilson, M., Humphreys, E.R., O'Hara, M.J., 2011. The Origin of Intra-plate Ocean Island Basalts (OIB): the lid effect and its geodynamic implications. Journal of Petrology 52, 1443–1468.
Pei, F.-P., Xu, W.-L., Yang, D.-B., Yu, Y., Wang, W., Zhao, Q.-G., 2011. Geochronology and geochemistry of Mesozoic mafic–ultramafic complexes in the southern Liaoning and southern Jilin provinces, NE China: constraints on the spatial extent of destruction of the North China Craton. Journal of Asian Earth Sciences 40, 636–650.
Peng, T., Wilde, S.A., Fan, W., Peng, B., 2013. Neoarchean siliceous high-Mg basalt (SHMB) from the Taishan granite-greenstone terrane, Eastern North China Craton: petrogenesis and tectonic implications. Precambrian Research 228, 233–249.
Pertermann, M., Hirschmann, M.M., 2003. Anhydrous partial melting experiments on MORB-like eclogite: phase relations, phase compositions and mineral–melt partitioning of major elements at 2–3 GPa. Journal of Petrology 44, 2173–2201.
Peslier, A.H., Woodland, A.B., Bell, D.R., Lazarov, M., 2010. Olivine water contents in the continental lithosphere and the longevity of cratons. Nature 467, 78–81.
Polat, A., Hofmann, A.W., Rosing, M.T., 2002. Boninite-like volcanic rocks in the 3.7–3.8 Ga Isua greenstone belt, West Greenland: geochemical evidence for intra-oceanic subduction zone processes in the early Earth. Chemical Geology 184, 231–254.
Polat, A., Herzberg, C., Münker, C., Rodgers, R., Kusky, T., Li, J., Fryer, B., Delaney, J., 2006. Geochemical and petrological evidence for a suprasubduction zone origin of Neoarchean (ca. 2.5 Ga) peridotites, central orogenic belt, North China craton. Geological Society of America Bulletin 118, 771–784.
Putirka, K.D., 2005. Mantle potential temperatures at Hawaii, Iceland, and the mid-ocean ridge system, as inferred from olivine phenocrysts: evidence for thermally driven mantle plumes. Geochemistry, Geophysics, Geosystems 6, Q05L08.
Putirka, K., Ryerson, F.J., Perfit, M., Ridley, W.I., 2011. Mineralogy and composition of the oceanic mantle. Journal of Petrology 52, 279–313.
Rhodes, J.M., Huang, S., Frey, F.A., Pringle, M., Xu, G., 2012. Compositional diversity of Mauna Kea shield lavas recovered by the Hawaii Scientific Drilling Project: inferences on source lithology, magma supply, and the role of multiple volcanoes. Geochemistry, Geophysics, Geosystems 13 Q03014.
Ridolfi, F., Renzulli, A., Puerini, M., 2010. Stability and chemical equilibrium of amphibole in calc-alkaline magmas: an overview, new thermobarometric formulations and application to subduction-related volcanoes. Contributions to Mineralogy and Petrology 160, 45–66.
Sobolev, A.V., Hofmann, A.W., Sobolev, S.V., Nikogosian, I.K., 2005. An olivine-free mantle source of Hawaiian shield basalts. Nature 434, 590–597.
Sobolev, A.V., Hofmann, A.W., Kuzmin, D.V., Yaxley, G.M., Arndt, N.T., Chung, S.-L., Danyushevsky, L.V., Elliott, T., Frey, F.A., Garcia, M.O., Gurenko, A.A., Kamenetsky, V.S., Kerr, A.C., Krivolutskaya, N.A., Matvienkov, V.V., Nikogosian, I.K., Rocholl, A., Sigurdsson, I.A., Sushchevskaya, N.M., Teklay, M., 2007. The amount of recycled crust in sources of mantle-derived melts. Science 316, 412–417.
Spandler, C., Yaxley, G., Green, D.H., Rosenthal, A., 2008. Phase relations and melting of anhydrous k-bearing eclogite from 1200 to 1600 degrees C and 3 to 5 GPa. Journal of Petrology 49, 771–795.
Spera, F.J., Bohrson, W.A., 2001. Energy-constrained open-system magmatic processes I: General model and energy-constrained assimilation and fractional crystallization (EC-AFC) formulation. Journal of Petrology 42, 999–1018.

Sturm, R., 2002. PX-NOM—an interactive spreadsheet program for the computation of pyroxene analyses derived from the electron microprobe. Computers & Geosciences 28, 473–483.
Sun, W., Ding, X., Hu, Y.-H., Li, X.-H., 2007. The golden transformation of the Cretaceous plate subduction in the west Pacific. Earth and Planetary Science Letters 262, 533–542.
Sun, S.-s., McDonough, W.F., 1989. Chemical and isotopic systematics of oceanic basalts: implications for mantle composition and processes. In: Saunders, A.D., Norry, M.J. (Eds.), Magmatism in the Ocean BasinsGeological Society, London, Special Publications 313–345.
Thompson, R.N., Gibson, S.A., 2000. Transient high temperatures in mantle plume heads inferred from magnesian olivines in Phanerozoic picrites. Nature 407, 502–506.
Wang, W., Xu, W.-l., Ji, W.-Q., Yang, D.-b., Pei, F.-p, 2006. Late Mesozoic and Palaeogene basalts and deep-derived xenocrysts in Eastern Liaoning Province, China: constraints on nature of lithospheric mantle. Geological Journal of China Universities 12, 30–40.
Wang, W., Xu, W.-l., Wang, D.-y., Ji, W.-q., Yang, D.-b., Pei, F.-p., 2007. Caiyuanzi Paleogene basalts and deep-derived xenocrysts in Eastern Liaoning, China: constraints on nature and deep process of the Cenozoic lithospheric mantle. Journal of Mineralogy and Petrology 27, 63–70.
Wang, X.C., Li, X.H., Li, W.X., Li, Z.X., Liu, Y., Yang, Y.H., Liang, X.R., Tu, X.L., 2008. The Bikou basalts in the northwestern Yangtze block, South China: remnants of 820–810 Ma continental flood basalts? Geological Society of America Bulletin 120, 1478–1492.
Wang, X.-C., Li, X.-H., Li, W.-X., Li, Z.-X., 2009. Variable involvements of mantle plumes in the genesis of mid-Neoproterozoic basaltic rocks in South China: a review. Gondwana Research 15, 381–395.
Wang, X.-C., Li, Z.-X., Li, X.-H., Li, J., Liu, Y., Long, W.-G., Zhou, J.-B., Wang, F., 2012. Temperature, pressure, and composition of the mantle source region of Late Cenozoic Basalts in Hainan Island, SE Asia: a consequence of a young thermal mantle plume close to subduction zones? Journal of Petrology 53, 177–233.
Wang, X.-C., Li, Z.-X., Li, X.-H., Li, J., Xu, Y.-G., Li, X.-H., 2013. Identification of an ancient mantle reservoir and young recycled materials in the source region of a young mantle plume: implications for potential linkages between plume and plate tectonics. Earth and Planetary Science Letters 377–378, 248–259.
Wang, X.-C., Li, Z.-X., Li, J., Pisarevsky, S.A., Wingate, M.T.D., 2014. Genesis of the 1.21 Ga Marnda Moorn large igneous province by plume–lithosphere interaction. Precambrian Research 241, 85–103.
Windley, B.F., Maruyama, S., Xiao, W.J., 2010. Delamination/thinning of sub-continental lithospheric mantle under Eastern China: the role of water and multiple subduction. American Journal of Science 310, 1250–1293.
Wu, F.-Y., Lin, J.-Q., Wilde, S.A., Zhang, X.O., Yang, J.-H., 2005a. Nature and significance of the Early Cretaceous giant igneous event in eastern China. Earth and Planetary Science Letters 233, 103–119.
Wu, F.-Y., Yang, J.-H., Wilde, S.A., Zhang, X.-O., 2005b. Geochronology, petrogenesis and tectonic implications of Jurassic granites in the Liaodong Peninsula, NE China. Chemical Geology 221, 127–156.
Wu, F.-Y., Walker, R.J., Yang, Y.-H., Yuan, H.-L., Yang, J.-H., 2006. The chemical-temporal evolution of lithospheric mantle underlying the North China Craton. Geochimica et Cosmochimica Acta 70, 5013–5034.
Wu, F., Xu, Y., Gao, S., Zheng, J., 2008. Controversy over studies of the lithospheric thinning and cratonic destruction of North China. Acta Petrologica Sinica 24, 1145–1174.
Xia, Q.-K., Liu, J., Liu, S.-C., Kovács, I., Feng, M., Dang, L., 2013. High water content in Mesozoic primitive basalts of the North China Craton and implications on the destruction of cratonic mantle lithosphere. Earth and Planetary Science Letters 361, 85–97.
Xu, Y.G., 2001. Thermo-tectonic destruction of the Archaean lithospheric keel beneath the Sino-Korean craton in China: evidence, timing and mechanism. Physics and Chemistry of the Earth, Part A: Solid Earth and Geodesy 26, 747–757.
Xu, Y., 2002. Evidence for crustal components in the mantle and constraints on crustal recycling mechanisms: pyroxenite xenoliths from Hannuoba, North China. Chemical Geology 182, 301–322.
Xu, Y.-G., 2014. Recycled oceanic crust in the source of 90–40 Ma basalts in North and Northeast China: evidence, provenance and significance. Geochimica et Cosmochimica Acta 143, 49–67.
Xu, Y.-G., Bodinier, J.-L., 2004. Contrasting enrichments in high- and low-temperature mantle xenoliths from Nushan, Eastern China: results of a single metasomatic event during lithospheric accretion? Journal of Petrology 45, 321–341.
Xu, Y.G., Ma, J.L., Huang, X.L., Iizuka, Y., Chung, S.L., Wang, Y.B., Wu, X.Y., 2004. Early cretaceous gabbroic complex from Yinan, Shandong Province: petrogenesis and mantle domains beneath the North China Craton. International Journal of Earth Sciences 93, 1025–1041.
Xu, Y., Li, H., Pang, C., He, B., 2009. On the timing and duration of the destruction of the North China Craton. Chinese Science Bulletin 54, 3379–3396.
Xu, Y.-G., Zhang, H.-H., Qiu, H.-N., Ge, W.-C., Wu, F.-Y., 2012. Oceanic crust components in continental basalts from Shuangliao, Northeast China: derived from the mantle transition zone? Chemical Geology 328, 168–184.
Xu, B., Charvet, J., Chen, Y., Zhao, P., Shi, G., 2013. Middle Paleozoic convergent orogenic belts in western Inner Mongolia (China): framework, kinematics, geochronology and implications for tectonic evolution of the Central Asian Orogenic Belt. Gondwana Research 23, 1342–1364.
Yang, W., Li, S., 2008. Geochronology and geochemistry of the Mesozoic volcanic rocks in Western Liaoning: implications for lithospheric thinning of the North China Craton. Lithos 102, 88–117.
Yang, J.-H., Chung, S.-L., Zhai, M.-G., Zhou, X.-H., 2004a. Geochemical and Sr–Nd–Pb isotopic compositions of mafic dikes from the Jiaodong Peninsula, China: evidence for vein-plus-peridotite melting in the lithospheric mantle. Lithos 73, 145–160.
Yang, J.-H., Wu, F.-Y., Chung, S.-L., Wilde, S.A., Chu, M.-F., 2004b. Multiple sources for the origin of granites: Geochemical and Nd/Sr isotopic evidence from the Gudaoling granite and its mafic enclaves, northeast China. Geochimica et Cosmochimica Acta 68, 4469–4483.
Yang, J.-H., Chung, S.-L., Wilde, S.A., Wu, F.-y., Chu, M.-F., Lo, C.-H., Fan, H.-R., 2005. Petrogenesis of post-orogenic syenites in the Sulu Orogenic Belt, East China: geochronological, geochemical and Nd–Sr isotopic evidence. Chemical Geology 214, 99–125.
Yang, J.-H., Wu, F.-Y., Wilde, S.A., Liu, X.-M., 2007a. Petrogenesis of Late Triassic granitoids and their enclaves with implications for post-collisional lithospheric thinning of the Liaodong Peninsula, North China Craton. Chemical Geology 242, 155–175.
Yang, J.H., Sun, J.F., Chen, F., Wilde, S.A., Wu, F.Y., 2007b. Sources and petrogenesis of Late Triassic dolerite dikes in the Liaodong Peninsula: implications for post-collisional lithosphere thinning of the eastern North China Craton. Journal of Petrology 48, 1973–1997.
Yang, D., Xu, W., Pei, F., Wang, Q., Gao, S., 2008a. Chronology and Pb isotope compositions of Early Cretaceous adakitic rocks in Xuzhou–Huaibei area, central China: constraints on magma sources and tectonic evolution in the eastern North China Craton. Acta Petrologica Sinica 24, 1745–1758.
Yang, J.-H., Wu, F.-Y., Wilde, S.A., Belousova, E., Griffin, W.L., 2008b. Mesozoic decratonization of the North China block. Geology 36, 467–470.
Yang, J.-H., O'Reilly, S., Walker, R.J., Griffin, W., Wu, F.-Y., Zhang, M., Pearson, N., 2010. Diachronous decratonization of the Sino-Korean craton: geochemistry of mantle xenoliths from North Korea. Geology 38, 799–802.
Yang, D.-B., Xu, W.-L., Pei, F.-P., Yang, C.-H., Wang, Q.-H., 2012a. Spatial extent of the influence of the deeply subducted South China Block on the southeastern North China Block: constraints from Sr–Nd–Pb isotopes in Mesozoic mafic igneous rocks. Lithos 136–139, 246–260.
Yang, J.-H., Sun, J.-F., Zhang, J.-H., Wilde, S.A., 2012b. Petrogenesis of Late Triassic intrusive rocks in the northern Liaodong Peninsula related to decratonization of the North China Craton: Zircon U–Pb age and Hf–O isotope evidence. Lithos 153, 108–128.
Ying, J., Zhang, H., Tang, Y., Su, B., Zhou, X., 2013. Diverse crustal components in pyroxenite xenoliths from Junan, Sulu orogenic belt: implications for lithospheric modification invoked by continental subduction. Chemical Geology 356, 181–192.
Yu, S.-Y., Xu, Y.-G., Ma, J.-L., Zheng, Y.-F., Kuang, Y.-S., Hong, L.-B., Ge, W.-C., Tong, L.-X., 2010. Remnants of oceanic lower crust in the subcontinental lithospheric mantle: trace element and Sr–Nd–O isotope evidence from aluminous garnet pyroxenite xenoliths from Jiaohe, Northeast China. Earth and Planetary Science Letters 297, 413–422.
Zeng, G., Chen, L.-H., Hofmann, A.W., Jiang, S.-Y., Xu, X.-S., 2011. Crust recycling in the sources of two parallel volcanic chains in Shandong, North China. Earth and Planetary Science Letters 302, 359–368.
Zhang, H.F., Sun, M., Zhou, X.H., Fan, W.M., Zhai, M.G., Yin, J.F., 2002. Mesozoic lithosphere destruction beneath the North China Craton: evidence from major-, trace-element and Sr–Nd–Pb isotope studies of Fangcheng basalts. Contributions to Mineralogy and Petrology 144, 241–253.
Zhang, H.-F., Sun, M., Zhou, X.-H., Zhou, M.-F., Fan, W.-M., Zheng, J.-P., 2003. Secular evolution of the lithosphere beneath the eastern North China Craton: evidence from Mesozoic basalts and high-Mg andesites. Geochimica et Cosmochimica Acta 67, 4373–4387.
Zhang, H.-F., SUN, M., Zhou, M.-F., FAN, W.-M., Zhou, X.-H., Zhai, M.-G., 2004. Highly heterogeneous Late Mesozoic lithospheric mantle beneath the North China Craton: evidence from Sr–Nd–Pb isotopic systematics of mafic igneous rocks. Geological Magazine 141, 55–62.
Zhang, H.-F., Nakamura, E., Kobayashi, K., Ying, J.-F., Tang, Y.-J., 2010. Recycled crustal melt injection into lithospheric mantle: implication from cumulative composite and pyroxenite xenoliths. International Journal of Earth Sciences 99, 1167–1186.
Zhao, G., Wilde, S.A., Cawood, P.A., Sun, M., 2001. Archean blocks and their boundaries in the North China Craton: lithological, geochemical, structural and P–T path constraints and tectonic evolution. Precambrian Research 107, 45–73.
Zhao, Z.-F., Dai, L.-Q., Zheng, Y.-F., 2013. Postcollisional mafic igneous rocks record crust–mantle interaction during continental deep subduction. Scientific Reports 3. http://dx.doi.org/10.1038/srep03413.
Zheng, J., 2009. Comparison of mantle-derived matierals from different spatiotemporal settings: implications for destructive and accretional processes of the North China Craton. Chinese Science Bulletin 54, 3397–3416.
Zheng, Y., Wu, F., 2009. Growth and reworking of cratonic lithosphere. Chinese Science Bulletin 54, 3347–3353.
Zhu, G., Jiang, D., Zhang, B., Chen, Y., 2012a. Destruction of the eastern North China Craton in a backarc setting: evidence from crustal deformation kinematics. Gondwana Research 22, 86–103.
Zhu, R.-X., Yang, J.-H., Wu, F.-Y., 2012b. Timing of destruction of the North China Craton. Lithos 149, 51–60.
Zindler, A., Hart, S., 1986. Chemical geodynamics. Annual Review of Earth and Planetary Sciences 14, 493–571.